Cascade Reaction of Ethanol to Butadiene over Multifunctional Silica-Supported Ag and ZrO_2 Catalysts

Naomi Miyake[†], Gordon Brezicki[†], and Robert J. Davis[†*]

[†]Department of Chemical Engineering

University of Virginia

102 Engineer's Way

Charlottesville, VA 22904-4741, USA

*Author to whom correspondence should be addressed: rjd4f@virginia.edu

Abstract

Although butadiene is currently a by-product of naphtha cracking, interest in producing butadiene from bio-based ethanol has increased because of the lower environmental impact of the ethanol to butadiene reaction. This work explores a multifunctional catalyst system composed of silica-supported Ag and ZrO_2 used for the cascade reaction of ethanol to butadiene at 573 K. The Ag and ZrO_2 components were synthesized on separate support particles enabling characterization of each component without interference from the other. High selectivity to butadiene (65%) at high ethanol conversion (75%) was achieved with an appropriate ratio of Ag and ZrO_2 in the reactor. Silver catalyzed the initial dehydrogenation of ethanol to acetaldehyde while ZrO_2 catalyzed the C-C coupling and subsequent dehydration reactions. The silica-supported ZrO_2 exhibited superior selectivity relative to bulk ZrO_2 in the Ag-promoted ethanol to butadiene reaction. Results from Zr K-edge X-ray absorption spectroscopy and UV-Vis spectroscopy showed that ZrO_2 was highly dispersed on the silica support over a range of loadings. Infrared spectroscopy of adsorbed pyridine, CO, and CO_2, and kinetics of probe reactions 1-butene double bond isomerization, 2-propanol decomposition, and ethanol hydrogenation of acetone were used to compare the acid-base nature and chemical reactivity of silica-supported ZrO_2 to bulk ZrO_2.

Key Words: acid, base, Lebedev reaction, zirconia, ethanol coupling

Introduction

Butadiene (1,3-butadiene) is a chemical intermediate, commonly used in the production of rubber tires.[1,2,3,4] Currently, butadiene is produced as a byproduct of naphtha cracking to ethene. With the reduced cost of natural gas in the past decade resulting from hydraulic fracturing, many hydrocarbon steam crackers switched to ethane as a feedstock. Cracking of ethane instead of naphtha produces fewer byproducts (e.g., propene, butadiene) during the cracking process. Thus, interest in alternative processes to produce butadiene has increased recently.

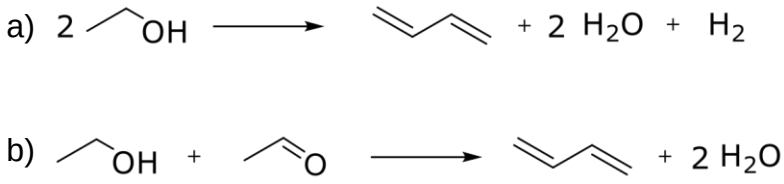

Scheme 1. a) Butadiene formation directly from ethanol in the Lebedev reaction. b) Butadiene formation from ethanol and acetaldehyde in the Ostromislensky reaction.

Butadiene can be produced from ethanol or a mixture of ethanol and acetaldehyde in a process known as the Lebedev reaction or the Ostromislensky reaction, respectively, as depicted in Scheme 1. Recent studies evaluating the environmental impacts of butadiene production via naphtha cracking versus ethanol conversion illustrate the overall benefits of ethanol-based processes.[5,6] Patel et al. showed that although the naphtha process is economically the better option with current technology, the environmental impact was significantly higher.[5] The naphtha-based process emitted more greenhouse gases (the equivalent of 1.5 kg CO_2/kg butadiene more) compared to the ethanol-based process. For context, the production of butadiene currently releases 180-200 million tons of CO_2 worldwide.[6] Shylesh et al. showed that, using their ethanol-based process, greenhouse gas emission could be reduced by 155%, compared to the traditional naphtha-based process.[7]

Results from Cespi et al. also showed that the Lebedev reaction compared with the naphtha-based process and the Ostromislensky reaction, had a lower environmental burden.[6] In addition to the overall environmental impact, the operational cost of the Lebedev process was lower than that of the Ostromislensky process. As a feedstock, ethanol derived from biomass has long been considered an effective alternative for fossil fuel-based processes.[8–10] Evidently, the direct conversion of ethanol to butadiene by the Lebedev reaction is the most likely of the ethanol-based processes to be commercialized, if the efficiency can be improved.

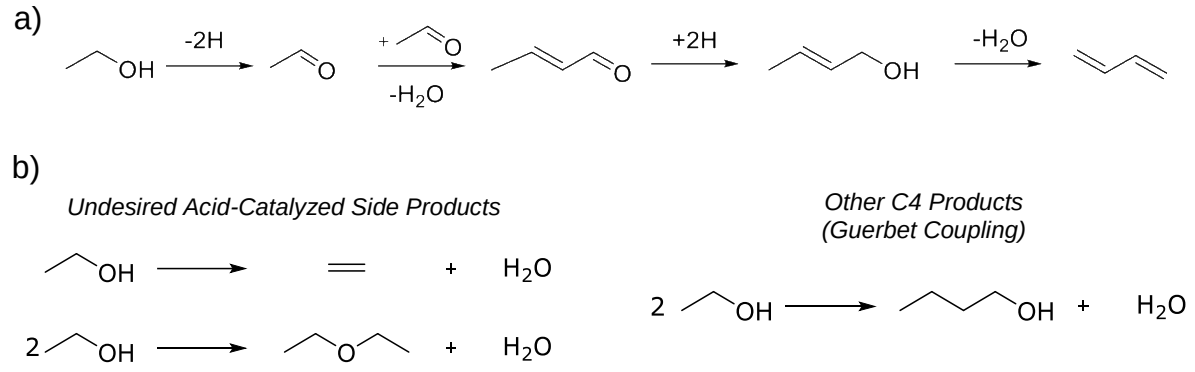

Scheme 2. a)Proposed reaction mechanism for the formation of butadiene from ethanol in the Lebedev reaction. b)Potential side products formed in the Lebedev reaction. Undesired acid-catalyzed reactions dehydrate ethanol forming ethene and diethyl ether. Ethanol can also undergo Guerbet coupling forming butanol instead of butadiene.

The most widely accepted reaction mechanism for the Lebedev reaction is composed of cascading steps depicted in Scheme 2a, facilitated by a multifunctional catalyst.[11] Initially, ethanol is dehydrogenated to form acetaldehyde. The acetaldehyde undergoes self-aldol condensation to crotonaldehyde, followed by hydrogenation to crotyl alcohol. Finally, the crotyl alcohol is dehydrated to the final product, butadiene. Common by-products include diethyl ether, ethene, and butanol (Scheme 2b). Diethyl ether and ethene result from the acid-catalyzed dehydration, instead of dehydrogenation, of ethanol. Butanol can be formed via a similar cascade reaction known as Guerbet coupling, involving the sequential

hydrogenation of the reaction intermediate crotonaldehyde to product butanol. Based on the acid-base nature of the multifunctional Lebedev catalyst, undesired acid-catalyzed by-products and butanol formation can be minimized.

The original Lebedev catalyst was a bifunctional mixed metal oxide that catalyzed both dehydrogenation and dehydration.[2] Toussaint and co-workers studied mixed metal oxides supported on silica as catalysts for the Ostromislensky reaction and found that Ta_2O_5 supported on SiO_2, followed closely by ZrO_2 on SiO_2, exhibited the best overall performance.[12] A small amount of metal promoter such as Cd or Cu was necessary to achieve high butadiene yield. Among the extensive number of catalysts studied by Natta and Rigamonti, a mixture of CuO, Ta_2O_5, and SiO_2 proved to be the most efficient catalyst in the Ostromislensky reaction.[13]

More recently, Jones et al. found that a mixture of Cu, Zn, and ZrO_2 supported on SiO_2 used in the Lebedev reaction had a relatively high selectivity of 67% towards butadiene but the conversion was less than 50%.[14] Prillaman et al. observed an increase in selectivity towards butadiene when ZrO_2 was added to their calcium phosphate catalyst in the Lebedev reaction.[11] Several groups have also observed an increase in butadiene yield over their MgO and SiO_2 catalyst with the addition of transition metals such as Ag and Cu.[15,16,17] Petrolini et al. showed that the addition of Cu to their AlMgO catalyst increased selectivity towards acetaldehyde while slowing the formation of diethyl ether.[18] In short, catalysts exposing both acid and base sites on their surface, typically obtained using mixed metal oxide systems, appear to effectively catalyze the Lebedev reaction. Adding a metal component, such as Ag or Cu, enhances the observed reaction rates over the metal oxide catalysts. In particular, a catalyst studied by Sushkevich et al. and by Dagle et al. composed of ZrO_2 and Ag supported

on SiO_2 exhibited the highest yield reported for a catalyst in the Lebedev reaction (70% selectivity towards butadiene at conversions >75%).[19,20]

A metal such as Ag is known to catalyze the dehydrogenation of ethanol to acetaldehyde and previous studies have shown that the particle size and loading of the Ag affects the conversion of ethanol to acetaldehyde.[21] Silver supported on SiO_2 with an average particle size of 1.9±0.8 nm proved to be more selective towards acetaldehyde compared to larger silver particles (3.2±1.6 nm). In addition, the overall conversion of ethanol in the presence of both Ag and ZrO_2 correlated with the loading of Ag in the reactor while the loading of ZrO_2 dictated the final product selectivity. Dagle et al. found that increasing ZrO_2 content from 4% to 18% on a $Ag/ZrO_2/SiO_2$ catalyst while maintaining the Ag loading had little to no effect on the overall ethanol conversion.[19] However, the selectivity towards butadiene seemed to slightly decrease (<10%) with increased ZrO_2 loading while the selectivity towards diethyl ether and ethene increased.

Zirconia is an amphoteric oxide, exposing both acidic and basic sites on its surface.[22,23,24] Depending on the synthesis method, the crystalline structure of ZrO_2 can be monoclinic, tetragonal, cubic, or a mixture of phases. Based on the local coordination environment around Zr, the catalytic rate for the same reaction can change depending on the phase of ZrO_2. For example, in the synthesis of methanol from CO_2/CO and H_2, Jung and Bell studied Cu supported on monoclinic and tetragonal ZrO_2.[25] They found that independent of CO_2 or CO reacting with H_2 and a similar Cu dispersion, monoclinic ZrO_2 consistently had higher methanol synthesis activity compared to tetragonal ZrO_2. In the Lebedev reaction, the ZrO_2 phase on $Ag/ZrO_2/SiO_2$ is thought to catalyze the reaction of ethanol and acetaldehyde (formed from ethanol dehydrogenation on the Ag component) to butadiene.[26,27,28] Indeed, a

detailed mechanistic study of the reaction showed that, after the initial dehydrogenation, the reaction takes place on Zr Lewis acid sites.[26]

In this contribution, we seek to deconstruct the Ag-promoted silica-supported ZrO_2 catalyst for the Lebedev reaction to enable characterization of the Ag and ZrO_2 components without mutual interference of the components. To this end, a co-impregnated Ag and ZrO_2 supported on SiO_2 ($Ag/ZrO_2/SiO_2$) catalyst comparable to prior reports was synthesized and compared to the performance of a physical mixture of Ag supported on SiO_2 (Ag/SiO_2) and ZrO_2 supported on SiO_2 (ZrO_2/SiO_2). Ethanol conversion over Ag/SiO_2 produced acetaldehyde, confirming its role in the initial dehydrogenation reaction shown in Scheme 2a. Therefore, the focus of this work is on the structure and reactivity of the silica-supported ZrO_2 species that are critical for the C-C coupling and dehydration reactions required for butadiene formation. In particular, the structure of the supported ZrO_2 species was investigated using X-ray absorption spectroscopy at the Zr K-edge and UV-Vis spectroscopy. The acid-base nature of the supported ZrO_2 species was probed via FT-IR spectroscopy of adsorbed pyridine, CO, and CO_2 as well as the model catalytic probe reactions 1-butene double-bond isomerization, 2-propanol decomposition, and hydrogen transfer from ethanol to acetone. Results from these techniques are interpreted in light of the performance of the catalysts in the Lebedev reaction.

Experimental Section

Catalyst Synthesis

Silica-supported ZrO_2 and Ag samples were synthesized using incipient wetness impregnation. The desired amount of zirconium (IV) oxynitrate hydrate (Sigma-Aldrich, 99.99% trace metal basis) and/or silver nitrate (Sigma-Aldrich, ACS Reagent) was dissolved in distilled deionized (DDI) water then added dropwise to SiO_2 (Grace, Davisil 636, 35-60 mesh particle size). After impregnation, the samples were dried in air at room temperature overnight, then at 393 K for 1 h, followed by a thermal treatment in 100 cm^3 min^{-1} of flowing air at 883 K for 6 h. The resulting materials are denoted as $xAg/xZrO_2/SiO_2$, xAg/SiO_2, and $xZrO_2/SiO_2$ where x denotes the nominal weight percent of the metal or metal oxide.

Monoclinic ZrO_2 (Sigma-Aldrich, 99% trace metals basis), zirconium hydroxide (MEL), and tetragonal ZrO_2 doped with Y_2O_3 (Sigma Aldrich, 8 mol% yttria) were thermally treated in 100 cm^3 min^{-1} of flowing air for 6 h at 883 K before use. The resulting catalyst was sized to 106-180 μm before use. Because yttria is an active catalytic component in the Lebedev reaction, the Y-stabilized tetragonal ZrO_2 was used solely as a structural standard in X-ray absorption spectroscopy. Monoclinic ZrO_2 will be referred to as ZrO_2(M). The ZrO_2 resulting from the thermal treatment of zirconium hydroxide (MEL) will be referred to as ZrO_2(M+T) because X-ray diffraction (Figure S1) revealed a mixture of the monoclinic and tetragonal phase.

Catalyst Characterization

Elemental analysis was performed by Galbraith Labs (Knoxville, TN) using inductively coupled plasma optical emission spectroscopy (ICP-OES).

Surface area was determined from the N_2 physisorption isotherm at 77 K recorded on a Micromeritics ASAP 2020 using the BET method for analysis.

X-ray diffraction patterns were obtained on a Panalytical Empyrean X-Ray Diffractometer using Cu Kα radiation and a scan rate of 0.0895° s^{-1} over a 2θ range of 20–80°.

Raman spectroscopy was performed using a Renishaw Invia™ Confocal Raman microscope using a 514 nm laser.

Transmission electron micrographs were obtained on an FEI Titan 80-300 instrument operating at 300 kV. Samples were supported on a Cu-supported holey carbon grid.

The UV-Vis spectra were recorded on a Perkin Elmer Lambda 850+ UV-Vis spectrometer. The reflectance standard was polytetrafluoroethylene (Sigma Aldrich, powder, >40μm). Spectra were collected from 190 to 300 nm. Zirconia(M+T) was diluted in silica prior to collection because of its high absorption.

X-ray absorption spectroscopy (XAS) was performed on beamline 8-ID at the National Synchrotron Light Source II (NSLS-II) at Brookhaven National Laboratory. Spectra were measured at the Zr K-edge (17998 eV) and the energy was calibrated using a Zr reference foil. Catalysts were analyzed using the methods described in previous work and the Demeter software package.[29,30,31] Briefly, catalysts were loaded into a home-built in-situ cell[32] and held in place using quartz wool. Three samples were analyzed simultaneously using the multi-sample holder design and the moveable stage at NSLS-II beamline 8-ID. The temperature was ramped at 2 K min^{-1} and He (Mattson Ultra-High Purity) was supplied using

multiple mass flow controllers. Ethanol was introduced to the cell using a room-temperature saturator.

The diffuse reflectance infrared Fourier transform spectroscopy (DRIFTS) experiments were conducted on a BioRad FTS-60A FTIR spectrometer and a Bruker Vertex 70 FTIR spectrometer. Silica-supported samples were diluted with KBr (50 wt%) and placed in a Harrick DRIFTS reactor cell mounted in a Harrick Praying Mantis optical accessory. Zirconia was used as is, with no KBr diluent. To improve reflectance signals, all samples were ground to a fine powder. Helium (99.999%, GTS Welco) gas lines were purified upstream using an OMI purifier (Supelco). Carbon monoxide (99.9%, GTS Welco) was passed through a SiO_2 trap at 195 K to remove carbonyls. All samples were treated at 773 K for 1 h in 30 cm^3 min^{-1} flowing He before cooling to experimental temperatures.

Experiments with CO were performed on the BioRad instrument using KBr windows at 303 K. Samples were exposed to CO diluted in He (5 kPa CO) in a 30 cm^3 min^{-1} stream for 0.5 h. Spectra were recorded in the presence of CO and gas-phase CO was subtracted from the spectra to isolate features due to adsorbed CO.

Pyridine (Sigma Aldrich, anhydrous, 99.8%) adsorption experiments were conducted on the Vertex instrument using ZnSe windows. Helium was passed at 5 cm^3 min^{-1} through a pyridine saturator maintained at 273 K. The stream of He and pyridine was further diluted by 25 cm^3 min^{-1} He before entering the DRIFTS cell. Samples were exposed to the pyridine/He mixture for 0.5 h at 373 K. Spectra were collected after purging the cell with He flowing at 30 cm^3 min^{-1} for 2 to 6 h, depending on the sample.

Experiments using CO_2 (GTS-Welco, 99.9%) used the Vertex instrument with ZnSe windows. Flowing CO_2 was diluted in He (2 kPa CO_2) in a 30 cm^3 min^{-1} stream and passed

over the sample at 303 K for 0.5 h. Temperature-programmed desorption was performed from 303 K to 573 K in 30 cm^3 min^{-1} of flowing He.

Catalytic Reactions

Anhydrous ethanol (Sigma Aldrich, 99.99%) was reacted in a downward flow, packed bed, titanium tubular reactor. Ethanol was fed to the system via a syringe pump connected to a vaporizer, producing a reactant stream composed of ethanol (6 kPa) balanced by N_2 (GTS-Welco, 99.999%). Methane (GTS-Welco, 99.97%) was added to the product stream as an internal standard for gas chromatography. The reaction temperature was 573 K for all ethanol to butadiene reactions.

The conversion and product selectivity were calculated based on the total amount of carbon present in the ethanol and product stream. Thus, overall conversion of ethanol based on product analysis was calculated as follows:

$$conversion\ (C\%) = \frac{\sum n_i M_i}{n_0 M_0} \times 100 \qquad (1)$$

where M_i is the molar flow rate of product i, M_0 is the initial molar flow rate of the reactant, n_0 is the number of carbons in the reactant (n_0=2 for ethanol), and n_i is the number of carbons in product i. Product selectivity is defined as follows:

$$selectivity\ (C\%) = \frac{n_i M_i}{\sum n_i M_i} \qquad (2)$$

Double bond isomerization of 1-butene was performed in the same reactor setup as described above for the ethanol reaction. The flowing 1-butene (Sigma Aldrich, 99+%) was mixed with a balance of N_2 to achieve the desired 1-butene concentration at a reaction temperature ranging between 303 K and 373 K.

The decomposition of 2-propanol was conducted in the same reactor setup as described above. Liquid 2-propanol (Fisher Chemical, ≥99.5%) was pumped to a vaporizer, producing a reactant stream composed of 2-propanol balanced by flowing N_2 at atmospheric total pressure. Methane was added to the product stream as an internal standard. The reaction temperature was varied between 473 K and 553 K.

The Meerwein-Ponndorf-Verley (MPV)-like reduction of acetone (Sigma-Aldrich, 99.9%) to 2-propanol was performed using ethanol as the sacrificial hydrogen source in the same reactor setup as described above. Ethanol and acetone were combined (acetone to ethanol molar ratio fixed at 0.1) and fed to the reactor, balanced by flowing N_2 at atmospheric total pressure, to achieve the desired concentration. Methane was added to the product stream as an internal standard. Reactions were conducted at 473 K. As a comparison, acetone was hydrogenated with H_2. Pure H_2 (25 cm^3 min^{-1}) was passed through a saturator containing liquid acetone, submerged in a dry ice/acetone bath. The reaction temperature was also at 473 K.

Prior to reaction, catalyst beds containing Ag were pretreated for 1 h at 623 K in 30 cm^3 min^{-1} of flowing H_2 (GTS-Welco, 99.999%), then lowered to the reaction temperature. Catalysts composed only of metal oxides were pretreated for 1 h at 773 K in 100 cm^3 min^{-1} of flowing N_2, then lowered to the reaction temperature. The product composition was evaluated using an online Agilent 7890A gas chromatograph equipped with a flame-ionization detector and a PoraPLOT Q-HT column.

In order to compare the silica-supported ZrO_2 with the unsupported ZrO_2, rates were calculated based on the Zr atoms exposed on the catalyst surface. For ZrO_2/SiO_2, 100% of the Zr^{4+} was assumed to be available for reaction. A density of 8 Zr^{4+} atoms nm^{-2} on the surface

of the catalyst was assumed for unsupported ZrO_2 based on literature results.[22] The fraction of Ag exposed was estimated from the measured particle size (see Supporting Information).

Equilibrium conversion of ethanol to acetaldehyde (plus dihydrogen) was calculated using ASPEN PLUS. Calculations were done with a Gibbs reactor and the Redlich-Kwong-Soave equation of state and 100% selectivity of ethanol to acetaldehyde was assumed i.e., no side products were included. Results for a temperature range of 473 K to 673 K are presented in Figure S2. Sample calculations of the Weisz-Prater criterion, evaluating potential internal transport limitations for ethanol dehydrogenation over Ag/SiO_2, are included in the Supporting Information.

Results and Discussion

Nitrogen Physisorption, ICP-OES, XRD, and Raman Spectroscopy

The BET surface area, pore volume, and the composition of the catalysts used in this study are listed in Table 1. The generally observed small decrease in surface area and pore volume with added ZrO_2 on SiO_2 can be attributed to the extra mass of the ZrO_2 on the

Table 1. Surface area, pore volume, and composition of catalysts.

Catalyst*	Surface Area ($m^2 g^{-1}$)	Pore Volume ($cm^3 g^{-1}$)	Nominal Zr Loading (wt %)	ICP-OES Results (wt %)
ZrO_2(M)	8.0	0.014	-	-
ZrO_2(M+T)	110	0.36	-	-
SiO_2	500	0.83	-	-
1Ag/SiO_2	430	0.82	-	Ag– 1.0
2ZrO_2/SiO_2	460	0.85	1.5	Zr – 1.2
4ZrO_2/SiO_2	460	0.86	3.0	Zr – 2.6
8ZrO_2/SiO_2	440	0.79	6.0	Zr – 5.5
16ZrO_2/SiO_2	390	0.71	12	Zr – 10
20ZrO_2/SiO_2	390	0.73	15	Zr – 13
1Ag/4ZrO_2/SiO_2	450	0.77	- 3.0	Ag – 0.9 Zr – 2.7

*xAg and $x$$ZrO_2$ are nominal composition

support instead of structural collapse of the silica.

Nominal Zr loading (wt %) was derived from the nominal ZrO_2 weight percentage based on the amount of ZrO_2 precursor used in synthesis. Compositions from ICP-OES matched well with the nominal compositions.

Catalysts were evaluated for crystalline phase using X-ray diffraction (XRD) and Raman spectroscopy (Figure S1). Even at the highest loading of ZrO_2, both XRD patterns and Raman spectra of the silica-supported ZrO_2 samples lacked features associated with crystalline ZrO_2, indicating the supported ZrO_2 phase was amorphous. Gao et al. found that the deposition of ZrO_2 on SiO_2 using incipient wetness resulted in no spectral change in Raman spectroscopy, attributing the lack of change to a high dispersion of ZrO_2.[33] Our

1Ag/SiO_2 sample also showed no distinct features in the XRD pattern, which is consistent with very small Ag nanoparticles in the nanometer size range.

Transmission Electron Microscopy

A representative dark-field TEM image of the 1Ag/SiO_2 catalyst is shown in Figure 1(a) and the particle size distribution is presented in Figure 1(b). The average particle size of the Ag was 1.8±0.5 nm, consistent with the 1.9±0.8 nm Ag particle sizes observed by Akhade et al. for a 1Ag/4ZrO_2/SiO_2 catalyst also prepared using incipient wetness impregnation on the same type of SiO_2 (Davisil 636).[21]

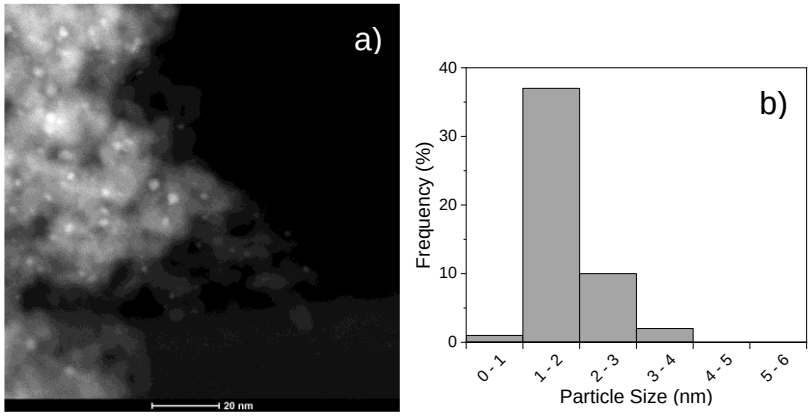

Figure 1. (a) Dark-field TEM image of 1Ag/SiO_2. (b) Particle size distribution of Ag on the 1Ag/SiO_2 catalyst.

UV-Vis Spectroscopy

The UV-Vis spectra of representative ZrO_2/SiO_2 samples compared to unsupported ZrO_2 are shown in Figure 2 and the corresponding absorption maxima and band gap energies (E_g) are listed in Table 2. A sample Tauc plot used to calculate E_g is included in the Supporting Information together with spectra of $20ZrO_2/SiO_2$ and the silica support. As the loading of silica-supported ZrO_2 increased, the absorption maximum shifted from 203 nm to 220 nm and the band gap shifted from 5.4 to 5.3 eV. The higher band gap of the low-loaded, silica-supported ZrO_2 sample (5.4 eV) relative to bulk ZrO_2 (5.0-5.2 eV) is the consequence of the well-known quantum size effect of semiconductor particles and confirms the highly dispersed nature of supported ZrO_2. The monoclinic ZrO_2 had a band maximum at 233 nm, while the band maximum for the ZrO_2(M+T) was at 227 nm. Zirconia is known to have two band-to-band transitions occurring at 238 nm and 214 nm for monoclinic ZrO_2.[34] Addition of tetragonal ZrO_2 tends to blue shift the feature at 238 nm. The difference in band maximum for tetragonal versus monoclinic ZrO_2 is well described in literature.[35,36] Therefore, it is not surprising that the band maximum reported in Figure 2b occurs at a higher wavelength for the monoclinic ZrO_2(M) compared to the mixed phase ZrO_2(M+T). Although the band maximum red shifted with increasing ZrO_2 content for the ZrO_2/SiO_2 samples, the band maximum for each of the two bulk ZrO_2 samples was at a higher wavelength than that of $16ZrO_2/SiO_2$. These results indicate that the supported ZrO_2 is highly dispersed on the surface of the SiO_2, but approaches a more crystalline form at higher loadings of ZrO_2.[35,33]

Table 2. Band maximum and band gap energy from UV-Vis spectra of ZrO_2/SiO_2 and bulk ZrO_2.

Sample	Band Max (nm)	Band gap Energy (eV)
$4ZrO_2/SiO_2$	203	5.4
$8ZrO_2/SiO_2$	208	5.3
$16ZrO_2/SiO_2$	210	5.3
ZrO_2 (M+T)	227	5.2
ZrO_2(M)	233	5.0

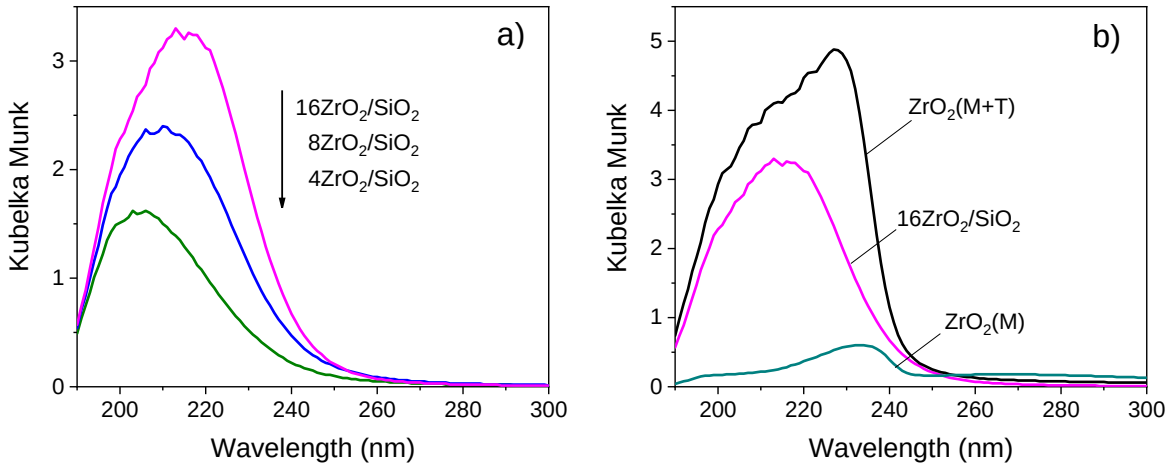

Figure 2. UV-Vis spectra of ZrO_2 and ZrO_2/SiO_2 evaluated at ambient conditions. (a)Comparison of $4ZrO_2/SiO_2$, $8ZrO_2/SiO_2$, and $16ZrO_2/SiO_2$. (b)Comparison of $16ZrO_2/SiO_2$, ZrO_2(M), and ZrO_2(M+T) spectra.

X-Ray Absorption Spectroscopy

In-situ X-ray absorption spectroscopy (XAS) was conducted on catalysts with different ZrO_2 loadings to study the change in Zr environment with respect to ZrO_2 loading and thermal treatment. Figure 3 shows the Zr K-edge X-ray absorption near edge structure (XANES) of catalysts with different ZrO_2 loadings compared with monoclinic and tetragonal ZrO_2. The spectra of the unsupported ZrO_2 samples are consistent with the monoclinic and tetragonal Zr K-edge XANES reported previously.[37,38,39] Monoclinic and tetragonal ZrO_2 have Zr cations in 7-fold and 8-fold coordination with O anions, respectively. The so-called white line at the absorption threshold of the monoclinic ZrO_2 is composed of a single broad peak whereas the white line region of the spectrum for tetragonal ZrO_2, has two overlapping peaks, characteristic of 8-fold coordination. Although the tetragonal ZrO_2 was doped with Y_2O_3, Li et al. showed that characteristic features in Zr XANES depends on the crystalline phase but

not on dopant.[38] All catalysts and bulk metal oxides have a similar K-edge energy characteristic of the Zr^{4+} oxidation state.[37,38,40]

For the lowest loading of 2 wt% ZrO_2, the Zr XANES revealed a white line absorption

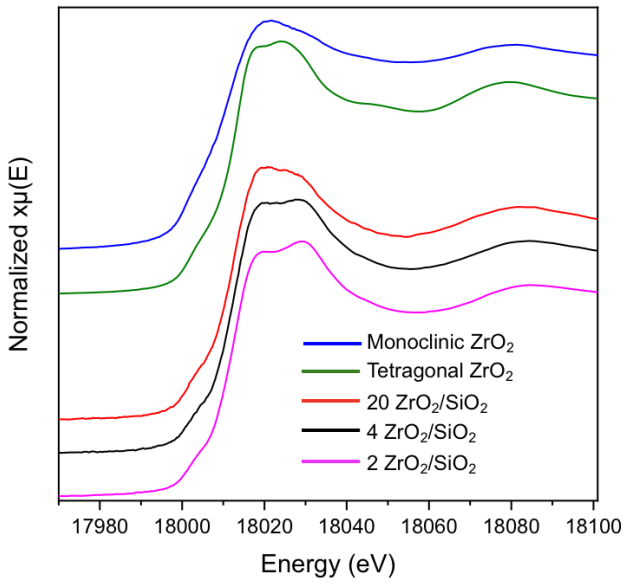

Figure 3. Results of XANES at the Zr K-edge for $2ZrO_2/SiO_2$, $4ZrO_2/SiO_2$, $20ZrO_2/SiO_2$, tetragonal ZrO_2, and monoclinic ZrO_2. Peaks are offset for comparison purpose.

feature composed of two broad peaks at 18018 eV and 18029 eV, with the higher energy feature being slightly more intense. As the loading of ZrO_2 increased, the ratio of intensities of these two peaks changed, with the peak at 18029 eV decreasing in intensity relative to that at 18018 eV. Mountjoy et al. observed a similar ratio change in relative intensity for the peaks at 18029 eV and 18018 eV with increased loading of ZrO_2 while studying zirconia-silica xerogels.[37] They argued that the evident change in relative intensities of the two peaks at 18018 eV and 18029 eV strongly suggests the existence of two Zr environments.

Figure 4 shows *in situ* XANES spectra for 2 wt% ZrO_2 on silica at different temperatures. At room temperature, no pre-edge feature was observed but as the temperature increased, a pre-edge feature at 18004 eV began to appear. The appearance of the pre-edge feature indicates that the Zr environment changed with heating to allow for a 1s to 4d transition. For certain ZrO_2 geometries, as the centrosymmetry is reduced, p-d mixing occurs, and therefore allows the 1s → 4d transition.[37,39] The appearance of this new feature could be in part due to the loss of adsorbed water molecules. At the same time, the main absorption peaks in the white line region changed with increased temperature. The relative peak intensity of the peak at 18029 eV increased while the peak at 18018 eV decreased. The introduction of ethanol at 623 K (Figure S5) showed a slight decrease in the pre-edge feature, possibly due to the adsorption of ethanol, re-introducing an -OH group, on some, but not all, of the Zr sites.

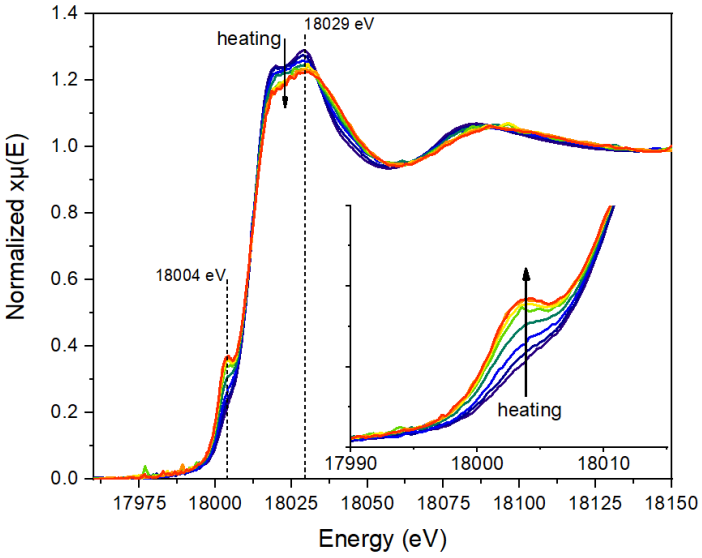

Figure 4. Normalized XANES at the Zr K-edge of $2ZrO_2/SiO_2$ heated from 298 K to 623 K in 30 cm^3 min^{-1} He.

The extended x-ray absorption fine structure (EXAFS) fitting parameters at the Zr K-edge for catalysts with different ZrO_2 loadings and at different temperatures are shown in Table 3. Figure S6 shows the corresponding magnitude and the imaginary part of the k^3-weighted FT-EXAFS. As reliable Zr-Si or Zr-Zr parameters could not be obtained, we limited our analysis to the first shell Zr-O only. At room temperature, the catalysts with various ZrO_2 loadings all exhibited a similar O coordination number of ~7.

However, after a thermal ramp to 623 K in He, the coordination of O to Zr decreased from 7 to 5 for $2ZrO_2/SiO_2$. Even with the introduction of ethanol at 623 K, the coordination number remained at 5. Previous studies show that it is typical for ZrO_2 mixed with SiO_2 to decrease in Zr-O coordination number with heating, most likely resulting from dehydroxylation.[37,40] With increasing temperature, the Debye-Waller factor (σ^2) decreased for $2ZrO_2/SiO_2$, which may seem counterintuitive at first. At higher temperature, however, the decrease in coordination number as well as the decrease in Zr-O bond length (R) from 2.04 to 2.01 Å may account for the observed decrease in the Debye-Waller factor.

Table 3. Fit for EXAFS parameters for $2ZrO_2/SiO_2$, $4ZrO_2/SiO_2$, and $20ZrO_2/SiO_2$ at 298 K in He. Results for $2ZrO_2/SiO_2$ at 623 K in He and in the presence of ethanol are also shown.

Catalyst	**Temperature (K)**	**R (Å)**	**N**	**σ^2 [Å^2]**
$2ZrO_2/SiO_2$	298 K	2.04 ± 0.03	7.0 ± 1.7	0.0058 ± 0.0042
$4ZrO_2/SiO_2$	298 K	2.08 ± 0.03	7.2 ± 1.5	0.0070 ± 0.0039
$20ZrO_2/SiO_2$	298 K	2.12 ± 0.03	7.2 ± 1.5	0.0059 ± 0.0039
$2ZrO_2/SiO_2$	623 K	2.01 ± 0.04	4.8 ± 1.5	0.0047 ± 0.0057
$2ZrO_2/SiO_2$ (EtOH)	623 K	2.01 ± 0.04	4.8 ± 1.5	0.0049 ± 0.0054

Diffuse Reflectance Infrared Fourier Transform Spectroscopy

Adsorption microcalorimetry of probe molecules triethylamine (TEA) and carbon dioxide was initially attempted to probe acid and base sites on the catalysts, respectively. Unfortunately, the uptakes and enthalpies of adsorption were inconclusive because of adsorption on the support (TEA, summarized in the Supporting Information) or insufficient signal intensities (CO_2, not shown). Thus, diffuse reflectance infrared Fourier transform spectroscopy (DRIFTS) of adsorbed pyridine, CO, and CO_2 was used to probe the surface acid and base sites.

Pyridine DRIFTS

Pyridine is commonly used to interrogate the acid sites on a catalyst, differentiating between Lewis and Brønsted acid sites since catalysts such as zirconia may expose both types of sites. Figure 5 shows the spectra of adsorbed pyridine on ZrO_2 and silica-supported ZrO_2 at 373 K. The spectra associated with the silica-supported ZrO_2 sample had features at 1448, 1488, 1576, and 1608 cm^{-1}, which are consistent with pyridine adsorbing on Lewis acid sites.[19,41,42] Brønsted acid sites interacting with pyridine to form pyridinium ions typically exhibit a prominent feature at 1540-1545 cm^{-1}.[19,41,42] Figure 6a and Figure 6b show the region between 1500 and 1560 cm^{-1} for pyridine on silica-supported ZrO_2 and on bulk ZrO_2, respectively. Although a very weak band at 1539 cm^{-1} appeared on the supported ZrO_2 catalysts at higher ZrO_2 loadings, the band may not be detectable on the samples with lower ZrO_2 loadings simply because of the low surface concentration of ZrO_2. Furthermore, the peak is very low in intensity, indicating that the Brønsted acid site density is likely negligible.

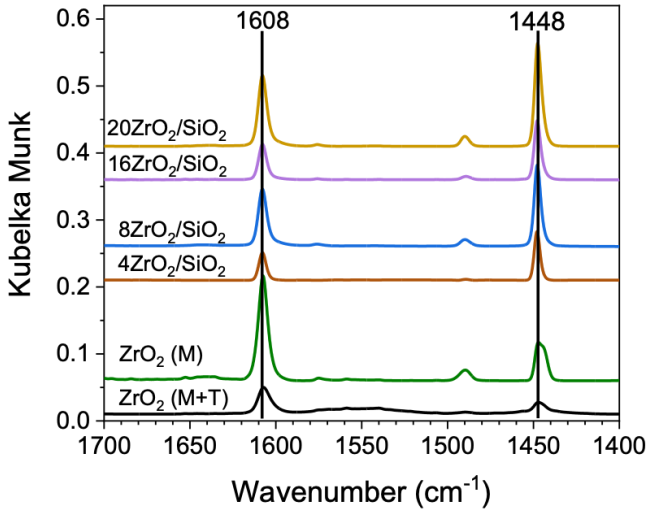

Figure 5. DRIFTS of adsorbed pyridine on ZrO_2(M+T), ZrO_2(M), $4ZrO_2/SiO_2$, $8ZrO_2/SiO_2$, $16ZrO_2/SiO_2$, and $20ZrO_2/SiO_2$ after purging with He at 373K. Peaks offset for clarity.

Li et al. also observed a feature at 1540 cm^{-1} on their 4 wt% silica-supported ZrO_2 catalyst prepared using incipient wetness impregnation.[43]

Pyridine adsorbed on ZrO_2(M) also had features at 1448, 1488, 1576, and 1608 cm^{-1}, characteristic of Lewis acid sites. The shoulder at 1443 cm^{-1} is most likely due to pyridine adsorbing on residual hydroxyl groups that remained after pretreatment. A trace amount of Brønsted acid sites might be present on the surface of ZrO_2(M), as indicated by the very weak feature at 1539 cm^{-1}, but feature intensity is barely above baseline. The higher intensity of the band at 1608 cm^{-1} compared to the band at 1448 cm^{-1} on ZrO_2(M) is consistent with results in literature.[41,43,44] The ZrO_2(M+T) has features similar to the ZrO_2(M). Indeed, the feature associated with Lewis acid sites at 1608 cm^{-1} has a higher intensity relative to the feature at 1448 cm^{-1} for ZrO_2(M+T). A very weak feature at 1539 cm^{-1} indicates that ZrO_2(M+T) also might possess a trace amount of Brønsted acid sites as indicated by the low intensity of the peak, in addition to Lewis acid sites, but nevertheless the ratio of Brønsted sites to Lewis sites is clearly very low.

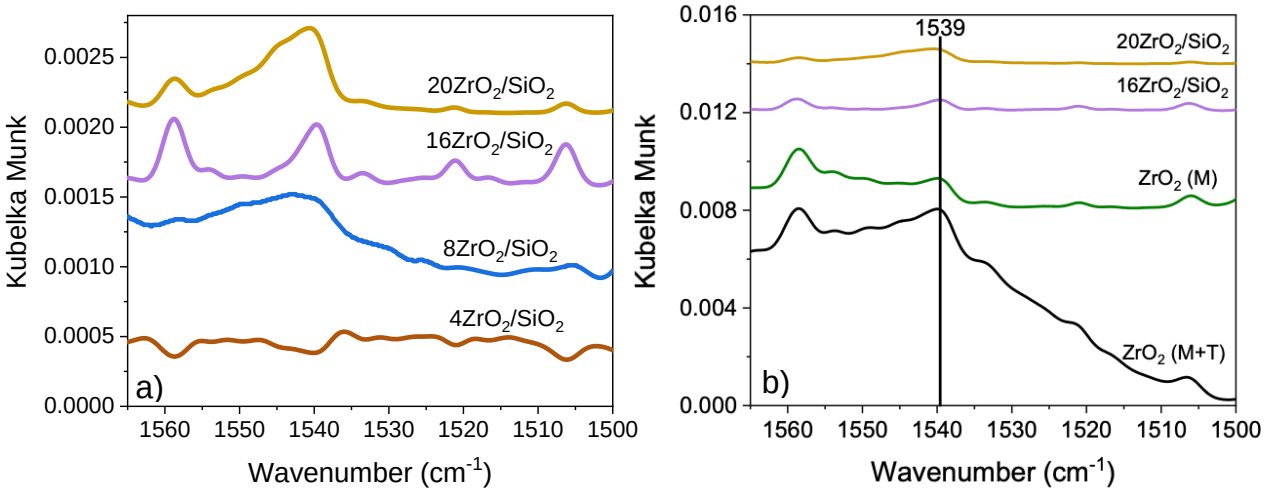

Figure 6. DRIFTS of adsorbed pyridine on ZrO_2 catalysts, specifically focusing on the region associated with Brønsted acid sites. (a)Comparison of silica-supported ZrO_2 (4 to 20 wt%). (b)Comparison of ZrO_2(M+T) and ZrO_2(M) with $16ZrO_2/SiO_2$ and $20ZrO_2/SiO_2$. Peaks offset for clarity.

Carbon Monoxide DRIFTS

As the Brønsted acid site density was very low on the catalysts, additional DRIFTS experiments focused on characterizing the Lewis acid sites on the catalysts. Carbon monoxide is a weak base and the interaction between CO and a Lewis acid site typically results in a blue shift of the CO absorption feature to a higher wavenumber relative to gas phase CO (2143 cm^{-1}).[45]

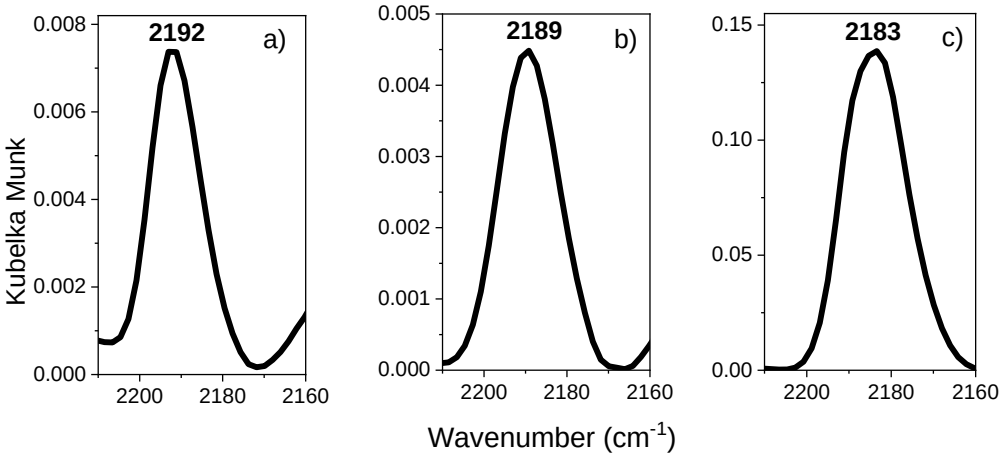

Figure 7. DRIFTS of CO adsorbed on (a)$4ZrO_2/SiO_2$, (b) monoclinic ZrO_2, and (c) monoclinic and tetragonal ZrO_2. Spectra were collected at 323 K in 5 kPa CO in He.

Carbon monoxide was adsorbed on bulk ZrO_2 and silica-supported ZrO_2 (ZrO_2 loadings between 4 and 20 wt%). As shown in Figure 7, adsorption of CO on ZrO_2(M) and ZrO_2(M+T) resulted in IR absorption bands of 2189 cm^{-1} and 2183 cm^{-1}, respectively, while the adsorption of CO on $4ZrO_2/SiO_2$ resulted in a band at 2192 cm^{-1} (Figure 7a), all of which are significantly blue shifted from the gas phase value of 2143 cm^{-1}. Carbon monoxide did not adsorb on SiO_2 under the studied conditions. Thus, the interaction between CO and the ZrO_2/SiO_2 catalysts is attributed to CO adsorbing on the coordinatively unsaturated Zr atoms. Even at higher ZrO_2 loadings (up to 20 wt%), the CO peak consistently appeared at 2192 cm^{-1}, suggesting that even with an increased density of Zr sites, the strength of CO interaction

with the individual Zr sites is similar (Figure S9). The peak associated with CO interacting with ZrO_2 in particular, is known to range between 2183 – 2200 cm^{-1} depending on the level of surface hydroxylation.[45,46] Therefore, the difference in CO peak position for unsupported ZrO_2 compared to ZrO_2/SiO_2 may simply be due to a difference in surface hydroxylation. Nevertheless, the results are consistent with similar Lewis acid interactions of CO with bulk and silica-supported zirconia.

Carbon Dioxide DRIFTS

Carbon dioxide is a weakly acidic molecule that it is commonly used to probe basic sites on metal oxide surfaces.[47] Adsorption of CO_2 on oxide surfaces forms different carbonate species. Previous studies show that various ZrO_2 polymorphs interact differently with CO_2 suggesting that the nature of basic sites depends on the phase of ZrO_2.[47] Adsorption of CO_2 followed by temperature-programmed desorption was performed on $4ZrO_2/SiO_2$ and bulk ZrO_2 as depicted in Figure 8 and Table 4 summarizes the peak assignments associated

Table 4. Peak assignments from DRIFTS for surface structures of adsorbed CO_2 on ZrO_2(M), ZrO_2(M+T), and ZrO_2/SiO_2.

Surface Structure	Peak Assignment (cm^{-1})		
	ZrO_2(M)	ZrO_2(M+T)	ZrO_2/SiO_2
bicarbonate (HCO_3)	1460	1420	1455
		1220	
bidentate bicarbonate (b-HCO_3)	1640	1630	
	1245		
bidentate carbonate (b-CO_3)	1562	1550	1600
		1340	
		1290	
monodentate carbonate (m-CO_3)	1480	1460	
	1398	1380	1395
	1380	1360	

with those spectra. Adsorption of CO_2 on $4ZrO_2/SiO_2$ at 303 K formed various carbonate species with features at 1600, 1455, and 1395 cm^{-1}. The bidentate carbonate feature at 1600 cm^{-1} was much larger than the monodentate carbonate feature at 1395 cm^{-1}. Increasing the temperature to 373 K resulted in a significant decrease in intensity of the peak at 1600 cm^{-1} and 1395 cm^{-1}. By 473 K, only a small peak associated with bidentate carbonate remained at 1600 cm^{-1} and at 573 K, nearly all the carbonate species had desorbed. The adsorption and desorption of CO_2 followed a similar pattern on the higher loaded $20ZrO_2/SiO_2$ sample (Figure S10).

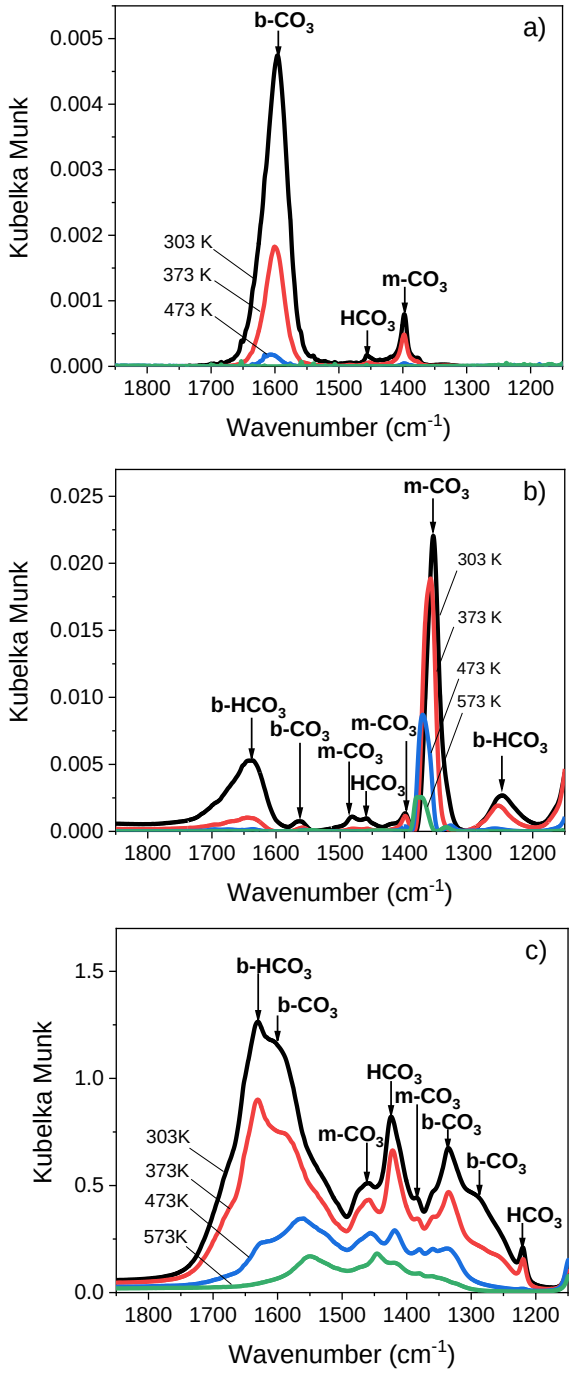

Figure 8. Temperature-programmed desorption of CO_2 from 303 K to 573 K on (a)$4ZrO_2/SiO_2$, (b)ZrO_2(M), and (c)ZrO_2(M+T).

A larger number of carbonate features was observed on bulk ZrO_2 compared to the silica-supported ZrO_2 catalysts. Regardless of the crystalline phase, bulk ZrO_2 formed bidentate carbonates (b-CO_3) and bidentate bicarbonates (b-HCO_3) in addition to monodentate bicarbonates (HCO_3) and monodentate carbonates (m-CO_3). The presence of bidentate carbonates could

suggest the existence of acid-base pairs on the surface of the catalyst, but it is unclear whether or not these acid-base pairs contribute to the catalytic activity. For ZrO_2(M), the monodentate carbonate feature was clearly the dominant feature while the bidentate bicarbonate and bidentate carbonate features were the most intense features on the ZrO_2(M+T). The difference between CO_2 DRIFTS associated with ZrO_2(M) and ZrO_2(M+T), suggests a significant difference on the surface oxides available for carbonate formation. Most importantly, for both unsupported ZrO_2 catalysts, carbonate species remained on their surfaces even after temperature-programmed desorption at 573 K. The higher thermal stability of the carbonates formed on the bulk ZrO_2 relative to silica-supported ZrO_2 was likely the result of stronger base sites associated with the bulk zirconia samples.

Ethanol Reaction on 1Ag/4ZrO_2/SiO_2

The ethanol reaction over the 1Ag/4ZrO_2/SiO_2 catalyst was carried out at 573 K. The catalytic performance was evaluated at different space velocities by varying the catalyst loading (Figure 9). At a low ethanol conversion of about 10%, the selectivity was primarily towards acetaldehyde, the initial dehydrogenation product of ethanol (Scheme 2). As the conversion increased, the selectivity towards butadiene also increased, which is consistent with the sequential nature of the cascade reaction involving acetaldehyde as an intermediate (Scheme 2). Thus, the high initial selectivity towards acetaldehyde (~70%) decreased to 5% at a high ethanol conversion (~80%). The selectivity towards the undesired acid-catalyzed side products diethyl ether and ethene remained relatively constant, around 15% at ethanol conversions less than 40%. At higher conversions (above 70%) the selectivity towards diethyl ether and ethene increased resulting in a maximum selectivity to butadiene of 65%

at an ethanol conversion of 75%, which is similar to the performance observed by Dagle et al. over a similar catalyst.[19]

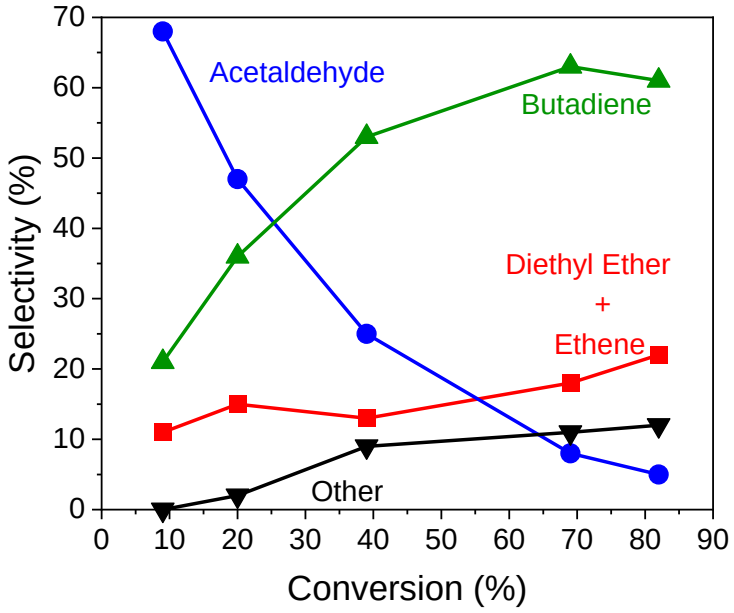

Figure 9. Product distribution over 1Ag/4ZrO_2/SiO_2 at 573 K at different space velocities. Other products include butanol, crotonaldehyde, butenes, C5+, and C6+ products. Reaction conditions: 6 kPa ethanol, 573 K.

Ethanol Dehydrogenation over 1Ag/SiO_2

The Ag/SiO_2 catalyzed the initial dehydrogenation of ethanol to acetaldehyde. Our kinetic studies of ethanol dehydrogenation over two different amounts of 1Ag/SiO_2 in the reactor as a function of ethanol partial pressure are summarized in Figure 10 and are consistent with a reaction order of about 0.6-0.7. Using FTIR spectroscopy, Sushkevich et al. concluded that the dehydrogenation reaction over Ag/SiO_2 was a first-order reaction.[48] It should be noted that ethanol dehydrogenation is quite rapid at 573 K and a Weisz-Prater analysis (Supporting Information) shows that the reaction is operating on the border of

intraparticle transport limitations. At 573 K and 6 kPa ethanol (standard conditions for the Lebedev reaction), the ethanol dehydrogenation turnover frequency (based on exposed Ag atom) is 0.032 s^{-1}.

Under the experimental conditions of 573 K and 1 atm of total pressure (6 kPa ethanol), assuming 100% selectivity to acetaldehyde, thermodynamic equilibrium calculations showed that the overall equilibrium conversion of ethanol was 97% (see Supporting Information). Garbarino et al. calculated a similar equilibrium conversion at 573 K, reporting 100% selectivity to acetaldehyde achieved at 700 K.[49,50] Indeed, experimental results (Table S1) show that an ethanol conversion of 98% can be achieved with a 91% selectivity towards acetaldehyde over the $1Ag/SiO_2$ catalyst.

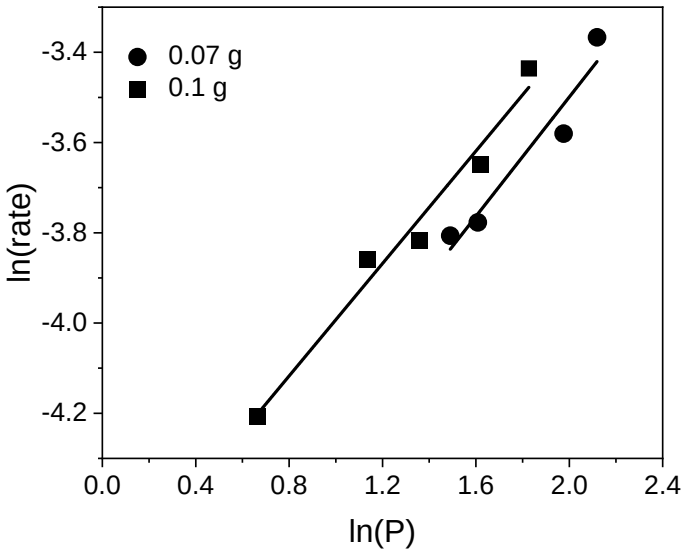

Figure 10. Rate of ethanol dehydrogenation over $1Ag/SiO_2$ on catalyst loadings of 0.07 g and 0.1 g at 573 K. Pressure is kPa, rate is mol (mol surface Ag)$^{-1}$ s^{-1}.

Ethanol Reaction Over Unsupported and Supported ZrO_2

To explore the contribution of the zirconia component of the catalyst, bulk ZrO_2 and silica-supported ZrO_2 were evaluated in the conversion of ethanol (Table 5). Monoclinic zirconia was unable to achieve a comparable conversion to $4ZrO_2/SiO_2$ under the experimental conditions because of its significantly lower surface area. Most importantly, the major products formed over the bulk ZrO_2 catalysts were the undesired ethanol dehydration side products diethyl ether and ethene. The rate of ethanol conversion (based on the surface Zr density), however, for the ZrO_2(M) was an order of magnitude lower than the rate for ZrO_2(M+T). Although the rates for the unsupported ZrO_2 were determined at different conversions (6.1% for ZrO_2(M) and ZrO_2(M+T) was 16%), the significant difference between the normalized rates allowed us to conclude that the ZrO_2(M+T) converted ethanol at a higher rate than purely monoclinic ZrO_2.

Table 5. Ethanol reaction over bulk and supported ZrO_2 catalysts.

Catalyst	Conversion (%)	Rate x10^{-3} (mol (mol Zr)$^{-1}$ s^{-1})	Selectivity (%)			
			DEE + Ethene[b]	AcH[b]	Butadiene	Other[b]
ZrO_2 (M) [a]	6.1	0.81	89	11	-	-
ZrO_2 (M+T)	16	10	78	11	5	6
$4ZrO_2/SiO_2$	10	0.75	90	10	-	-
$4ZrO_2/SiO_2$	17	0.43	93	6	-	1

[a]Lower conversion due to lower surface area
[b]DEE = diethyl ether, AcH = acetaldehyde, other = crotonaldehyde, butanol, butenes, C5+, C6+ products
Reaction conditions: 6 kPa ethanol, 573K

At a conversion of 17%, ethanol was dehydrated over $4ZrO_2/SiO_2$ to diethyl ether and ethene with a combined selectivity of 93%. The rate of reaction was 4.3 x10^{-4} mol (mol Zr)$^{-1}$ s^{-1}, significantly lower than the rate of reaction over ZrO_2(M+T) which had an ethanol reaction rate of 1.0x10^{-2} mol (mol Zr)$^{-1}$ s^{-1}. Monoclinic ZrO_2 and $4ZrO_2/SiO_2$, on the other

hand, had comparable rates ($8.1x10^{-4}$ mol (mol Zr)$^{-1}$ s^{-1} and $7.5x10^{-4}$ mol (mol Zr)$^{-1}$ s^{-1}, respectively) at comparable conversions of 6.1% for ZrO_2(M) and 10% for $4ZrO_2/SiO_2$.

Comparison of Ethanol Reaction with Physical Mixture and Co-Impregnated $1Ag/4ZrO_2/SiO_2$

To eliminate the potential modification of ZrO_2 surfaces by addition of the Ag promoter, the ethanol reaction was performed with a physical mixture of $1Ag/SiO_2$ and $4ZrO_2/SiO_2$ and results were compared to those obtained over co-impregnated Ag-promoted silica-supported ZrO_2 (Table 6). At a similar conversion of ethanol, the selectivity of both catalyst systems (physical mixture and co-impregnated) towards the acid-catalyzed side-products diethyl ether and ethene was similar over both catalysts. While the selectivity towards acetaldehyde was lower and the selectivity towards butadiene was higher over the physical mixture compared to the co-impregnated catalyst, this difference may be the result of slightly higher conversion, which is known to favor butadiene in the cascade reaction (Figure 9), over the physically mixed catalyst. Nevertheless, the co-impregnated catalyst and the physical mixture exhibited comparable catalytic performance, confirming that the Ag and ZrO_2 components can be present on separate support particles.

Table 6. Ethanol reaction over co-impregnated and physical mixture of silica-supported Ag and ZrO_2.

Catalyst	Conversion (%)	Selectivity (%)			
		DEE + Ethene[a]	AcH[a]	Butadiene	Other[a]
$1Ag/4ZrO_2/SiO_2$	20	15	47	36	2
$1Ag/SiO_2$ and $4ZrO_2/SiO_2$	25	14	35	49	2

[a]DEE = diethyl ether, AcH = acetaldehyde, other = crotonaldehyde, butanol, butenes, C5+, C6+ products
Reaction conditions: 6 kPa ethanol, 573 K

While the $4ZrO_2/SiO_2$ catalyst produced predominantly diethyl ether and ethene from ethanol (Table 5), the physical mixture of $4ZrO_2/SiO_2$ and $1Ag/SiO_2$ produced an appreciable amount of butadiene by the cascade reactions of ethanol dehydrogenation on the Ag component and the C-C coupling/dehydration reaction on the zirconia component. These results show that a critical balance must exist between the Ag and ZrO_2 components to effectively produce butadiene from ethanol, which is consistent with conclusions from other works.[19,20]

Ethanol Conversion at Different Mass Ratios of Ag and ZrO_2

In their study of supported Ag and ZrO_2 on SiO_2, Sushkevich et al. correlated Lewis acid site concentrations to the overall ethanol conversion.[27,28] In contrast, Dagle et al. showed that at the same space velocity, $4Ag/SiO_2$ and $4Ag/4ZrO_2/SiO_2$ had a similar conversion while $4ZrO_2/SiO_2$ had a much lower conversion.[19] They concluded that the Ag particles, not the Lewis acid sites, were responsible to a large extent for the overall ethanol conversion. To investigate the role of ZrO_2 and Ag on the overall conversion, physical mixtures of various

Table 7. Physical mixture of $1Ag/SiO_2$ and $4ZrO_2/SiO_2$ at different mass ratios in the ethanol reaction. $1Ag/SiO_2$ was kept constant at 0.2 g while $4ZrO_2/SiO_2$ was varied.

Entry	Catalyst	Mass Ratio	Conversion (%)	Selectivity (%)			
				DEE + Ethene[a]	AcH[a]	Butadiene	Other[a]
1	$1Ag/SiO_2$ and $4ZrO_2/SiO_2$	0.5	21	8	45	44	3
2	$1Ag/SiO_2$ and $4ZrO_2/SiO_2$	0.25	24	34	22	42	2
3	$1Ag/SiO_2$ and $8ZrO_2/SiO_2$	1	26	10	40	46	4

[a]DEE = diethyl ether, AcH = acetaldehyde, other = crotonaldehyde, butanol, butenes, C5+, C6+ products
Reaction conditions: 6 kPa ethanol, 573K

ratios of $1Ag/SiO_2$ and $4ZrO_2/SiO_2$ were compared. In particular, the mass of $1Ag/SiO_2$ was kept constant in the reactor while the mass of the physically mixed $4ZrO_2/SiO_2$ was varied. Results from those runs are presented in Table 7.

The first two entries of Table 7 show that increasing the ZrO_2 amount in the reactor by a factor of 2, at constant Ag loading, barely affected the conversion of ethanol, indicating that the ethanol dehydrogenation reaction controls ethanol conversion (at low conversion levels). The selectivity to products, however, was significantly affected by ZrO_2 loading, with the enhancement of undesirable acid-catalyzed dehydration reactions at higher loadings (Entry 2 in Table 7).

To explore the potential influence of ZrO_2 loading on the catalytic performance of the silica-supported ZrO_2 catalysts, the reaction of ethanol was carried out in a reactor loaded with Ag/SiO_2 physically mixed with either $4ZrO_2/SiO_2$ or $8ZrO_2/SiO_2$, while maintaining the same amount of Ag and ZrO_2 in the reactor (Entry 1 and 3 in Table 7). The similarity of the ethanol conversion and product selectivity for Entry 1 and 3 confirms that the performance of the silica-supported ZrO_2 is independent of the Zr surface density over the tested range.

Ethanol Reactions over Unsupported and SiO_2-Supported ZrO_2 Physically Mixed with $1Ag/SiO_2$

Physical mixtures of ZrO_2(M) and $1Ag/SiO_2$ were compared with physical mixtures of $4ZrO_2/SiO_2$ and $1Ag/SiO_2$ in the reaction of ethanol at 573 K and the results for similar ethanol conversion (~25%) are summarized in Figure 11. The ratio of Ag to ZrO_2 present in the physical mixture is shown as a ratio of Ag atoms to Zr atoms. We chose to explore in detail the reactivity of ZrO_2(M) instead of ZrO_2(M+T) as the latter catalyst dehydrates ethanol at a much higher rate (see Table 5). On $4ZrO_2/SiO_2$, 100% exposure of Zr atoms was assumed,

and the loading of Zr determined using ICP-OES was used to calculate the number of surface Zr atoms. For the unsupported, bulk ZrO_2(M), the number of surface Zr atoms was estimated by assuming a Zr surface density of 8 nm^{-2}.[22] The fraction of Ag exposed on $1Ag/SiO_2$ was assumed to be 0.65, based on the particle size derived from TEM. Additional information regarding the calculation of surface atom density can be found in the Supporting Information.

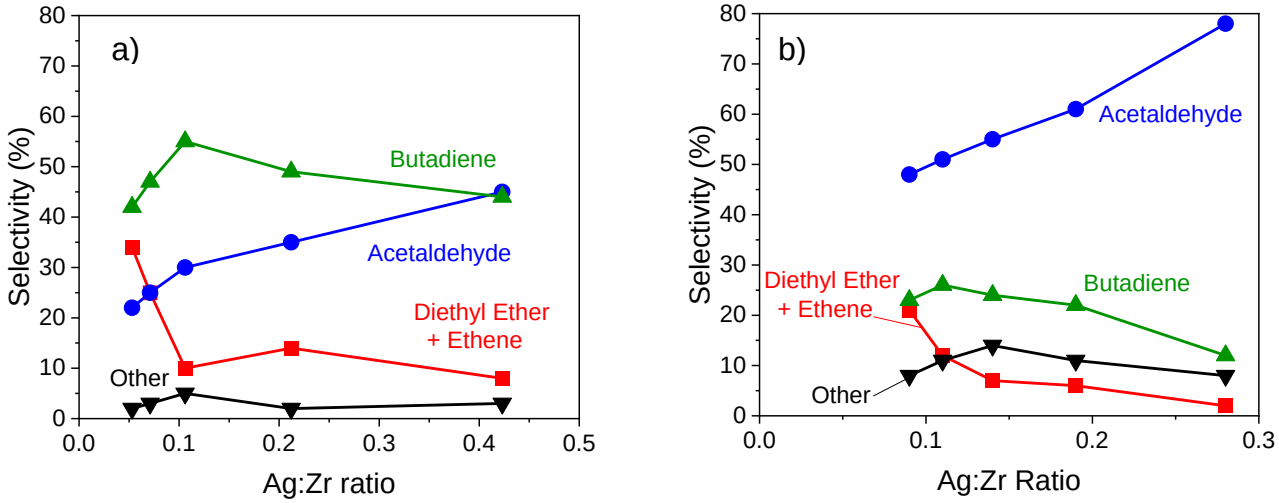

Figure 11. Product selectivity at different Ag to Zr ratios of (a)$1Ag/SiO_2$ and $4ZrO_2/SiO_2$ and (b)$1Ag/SiO_2$ and ZrO_2(M). Mass of $1Ag/SiO_2$ was kept constant at 0.2 g for $4ZrO_2/SiO_2$ and 0.4 g for ZrO_2(M). The mass of $4ZrO_2/SiO_2$ and ZrO_2(M) was varied. Other products include crotonaldehyde, butanol, butenes, C5+, and C6+ products. Conversion was constant at ~25% at 573 K and 6 kPa ethanol.

Figure 11a shows the difference in product ratio as the mass of $4ZrO_2/SiO_2$ was varied while the $1Ag/SiO_2$ mass was kept constant over an Ag to Zr atom ratio that ranged from 0.053 to 0.42. As expected, the selectivity towards acetaldehyde steadily decreases with additional ZrO_2 in the reactor because of the sequential reaction of acetaldehyde to butadiene. The highest ZrO_2 loadings (lowest Ag:Zr ratio) promoted the formation of the ethanol dehydration products ethene and diethyl ether. We observed a maximum in the butadiene selectivity at a mass ratio of 0.11, which demonstrates the sensitivity of the Lebedev reaction to the ratio of Ag metal sites and ZrO_2 sites in the reactor.

A similar set of reactions was conducted on physically mixed $1Ag/SiO_2$ and ZrO_2(M), shown in Figure 11b. Compared to the physical mixture of $4ZrO_2/SiO_2$ and $1Ag/SiO_2$, the selectivity towards butadiene was clearly lower over the mixture with bulk ZrO_2. Besides the quantitative difference in selectivity, the overall trend in product distribution was similar between the physical mixture of $1Ag/SiO_2$ with $4ZrO_2/SiO_2$ or ZrO_2(M). In particular, the selectivity towards butadiene achieved a maximum as the ratio of Ag to ZrO_2 was varied in the reactor. For ZrO_2(M), a maximum butadiene selectivity of 26% was achieved at an Ag to Zr ratio of 0.11 while the maximum butadiene selectivity was achieved at a ratio of 0.11 for $4ZrO_2/SiO_2$. Although the maximum selectivity to butadiene occurs at the same Ag to Zr ratio of 0.11, the significant difference in selectivity towards butadiene shows that the Zr environment (bulk versus supported) plays a key role in the selective production of butadiene. For comparison, a physical mixture of Ag/SiO_2 and ZrO_2(M+T) with Ag:Zr ratio of 0.041 revealed product selectivities to acetaldehyde (55%), butadiene (6%), other C4+ products (16%), and acid-catalyzed ethanol dehydration products (23%) at an ethanol conversion of 12%, which confirms the rather poor performance of ZrO_2(M+T) in the Lebedev reaction.

The difference in acetaldehyde/butadiene selectivity between the physical mixtures of Ag with bulk or supported ZrO_2, as summarized in Figure 11, suggests that the $4ZrO_2/SiO_2$ component is more effective than bulk ZrO_2 at catalyzing C-C bond formation of the intermediate acetaldehyde.

Additional Catalytic Probe Reactions

The surface acid and base sites on ZrO_2 catalysts can also be studied using probe reactions, such as 1-butene double bond isomerization and 2-propanol decomposition. The double bond of 1-butene can shift down the chain to form cis- and trans-2-butene over acid-base catalysts (Scheme 3a). Acid catalysts typically exhibit products with a cis-to-trans ratio close to 1 while more basic catalysts tend to form products with a higher cis-to-trans ratio.[51] Amphoteric oxides such as ZrO_2 tend to fall in between, revealing a cis-to-trans ratio higher than 1, but not as high as well-recognized basic oxides such as MgO.[51] The decomposition of 2-propanol yields acetone and propene (Scheme 3b) in different ratios depending on the acid and base sites on the catalyst surface.[52] Acetone is formed via the dehydrogenation of 2-propanol, typically associated with base catalysts, while propene is formed via dehydration of 2-propanol on acid catalysts. Diisopropyl ether can also be formed as the result of a bimolecular reaction between surface isopropoxide species.[53]

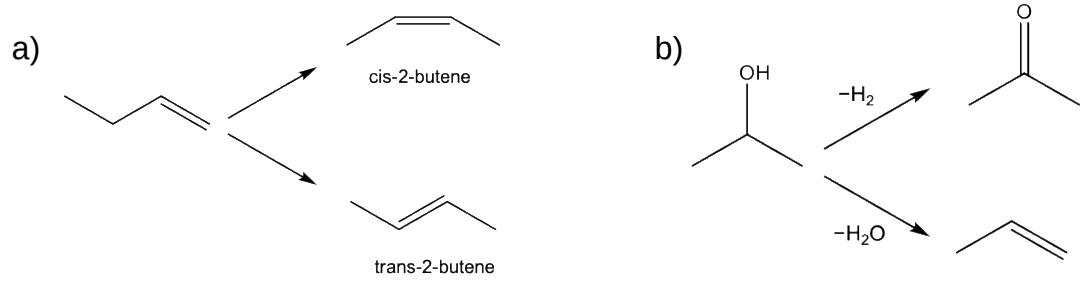

Scheme 3. a)Formation of cis- and trans-2-butene from the double bond isomerization of 1-butene. b)2-propanol decomposition to acetone and propene.

During the Guerbet reaction of ethanol to butanol, the hydrogenation of crotonaldehyde to crotyl alcohol (Scheme 2a) has been shown to most likely occur via the MPV-like transfer of hydrogen from ethanol to crotonaldehyde.[54,55] Studies of the

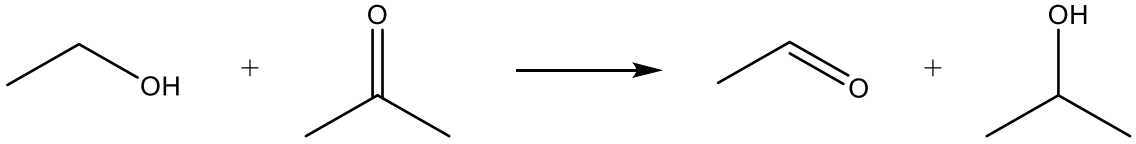

Scheme 4. The MPV-like hydrogen transfer from ethanol to acetone producing acetaldehyde and 2-propanol.

1Ag/4ZrO_2/SiO_2 catalyst in the context of the Lebedev reaction also suggest that hydrogenation of crotonaldehyde occurs via an MPV-like reaction with ethanol as the sacrificial alcohol.[56] Thus, the hydrogenation of acetone with ethanol can be used as a model reaction to study the MPV-like reaction over our ZrO_2 catalysts. Scheme 4 shows the MPV-like transfer of hydrogen from ethanol to acetone.

1-Butene Double Bond Isomerization Reaction

The 1-butene double bond isomerization reaction was evaluated over silica-supported ZrO_2 and unsupported ZrO_2. The initial conversion of 1-butene (space velocity adjusted to give conversions from 2 to 4%), the cis-to-trans ratio of the product 2-butenes, and rate observed over various silica-supported ZrO_2 catalysts are summarized in Table 8. Figure S11 shows that over the duration of the experiment, the conversion of 1-butene remained relatively stable over silica-supported ZrO_2. With increased ZrO_2 loading on silica, the cis-to-trans ratio of the product 2-butenes did not change, ranging between 1.3 and 1.5. Ozaki et al. also observed a cis-to-trans ratio of 1.2 for the reaction over supported ZrO_2 on SiO_2 at 298 K.[57] Comparing the results obtained over 4ZrO_2/SiO_2 and 20ZrO_2/SiO_2, the rate of the 1-butene isomerization reaction was 4.7×10^{-2} mol (mol Zr)$^{-1}$ s^{-1} and 3.1×10^{-2} mol (mol

Table 8. Performance of ZrO_2/SiO_2 catalysts in the 1-butene double bond isomerization reaction.

Catalyst	Conversion (%)	Cis-to-Trans Ratio	Rate x 10^{-2} (mol (mol Zr)$^{-1}$ s^{-1})
4ZrO_2/SiO_2	3.9	1.3	4.7
8ZrO_2/SiO_2	2.5	1.3	3.1
16ZrO_2/SiO_2	2.8	1.5	2.8
20ZrO_2/SiO_2	3.2	1.3	3.1

Reaction conditions: 2 kPa 1-butene, 373 K

$Zr)^{-1}$ s^{-1}, respectively. The relatively constant turnover rate per Zr (within 30%) when the Zr loading was increased by a factor of 5 and the consistent cis-to-trans ratio of the product 2-butenes (1.3 to 1.5) are consistent with silica-supported ZrO_2 samples examined in this work possessing highly dispersed ZrO_x species on the silica surface.

Temperature effects were also studied on $16ZrO_2/SiO_2$ from 323 K to 373 K (Table 9). As expected, the rate increased with increasing temperature from $4.1x10^{-3}$ mol (mol Zr)$^{-1}$ s^{-1} to $2.8x10^{-2}$ mol (mol Zr)$^{-1}$ s^{-1}. The cis-to-trans ratio, however, did not change significantly, increasing slightly from 1.3 at 323 K to 1.5 at 373 K.

The performance of bulk ZrO_2(M+T) was also evaluated in the 1-butene isomerization reaction. As deactivation was observed over ZrO_2(M+T) with time during the isomerization reaction (see Figure S12 for a time evolution of the reaction), a first order deactivation model (Eq. 3) was used to determine the initial conversion:

$$k_d = \frac{\ln\left(\frac{1-X_t}{X_t}\right) - \ln\left(\frac{1-X_0}{X_0}\right)}{t} \qquad (3)$$

where k_d is the deactivation coefficient, X_t is the conversion at time t, and X_0 is the initial conversion. Figure S12 shows that the model fits the experimental results relatively well.

The reaction over ZrO_2(M) and ZrO_2(M+T) was compared at the same reaction temperature of 373 K (Table 9). The 1-butene isomerization occurred at a much higher rate over the mixed phase ZrO_2 relative to the monoclinic ZrO_2. This difference in rate is nearly identical to that observed in the ethanol reaction over the two bulk zirconia samples (Table 5). The cis-to-trans ratio was substantially greater than 1 for both unsupported zirconias, 3.1 for ZrO_2(M+T) and 4.0 for ZrO_2(M) at 373 K. This cis-to-trans ratio falls within the values of reported cis-to-trans ratio observed over ZrO_2, which can range between 3 and 7 for ZrO_2

depending on preparation method and reaction temperature.[58] We suspect that the higher rates of ethanol dehydration and 1-butene double bond isomerization over ZrO_2(M+T) relative to ZrO_2(M) can be attributed to a higher surface defect density (i.e., higher density of low coordinated Zr surface sites) associated with the high surface area, mixed phase ZrO_2(M+T) sample.

Table 9. Influence of temperature on 1-butene double bond isomerization over bulk ZrO_2 and $16ZrO_2/SiO_2$.

Catalyst	Temperature (K)	Conversion (%)	Cis-to-Trans Ratio	Rate x 10^{-2} (mol (mol Zr)$^{-1}$ s^{-1})
ZrO_2(M+T)	313	8.2	5.8	8.6
ZrO_2(M+T)	323	9.9	5.4	12
ZrO_2(M+T)	353	10	3.8	44
ZrO_2(M+T)	373	11	3.1	69
ZrO_2(M)	373	7.6	4.0	4.6
$16ZrO_2/SiO_2$	323	2.9	1.3	0.40
$16ZrO_2/SiO_2$	353	4.4	1.3	1.1
$16ZrO_2/SiO_2$	373	2.6	1.3	3.2
$16ZrO_2/SiO_2$	393	3.4	1.3	6.2

Reaction conditions: 2 kPa 1-butene

The higher cis-to-trans ratio of product 2-butenes observed on ZrO_2(M) and ZrO_2(M+T) is often correlated with basic sites on catalysts. For example, a classic solid base such as MgO can form 2-butenes with a cis-to-trans ratio as high as 11 at 299 K.[59] As ZrO_2 is considered to be an amphoteric oxide, i.e., exposing both acid and base sites, it is not surprising that the cis-to-trans ratio was much higher than 1. The cis-to-trans ratio of silica-supported ZrO_2 catalysts being near unity is consistent with those materials exposing Lewis acid Zr atoms bonded to weakly basic oxygen atoms. Indeed, the weak basic strength of ZrO_2/SiO_2 inferred from the low temperature at which CO_2 desorbs during the TPD

experiment (see Figure 8a) is completely consistent with the results from 1-butene double bond isomerization.

Decomposition of 2-Propanol

To further probe the acid and base sites, the decomposition of 2-propanol was performed over bulk ZrO_2(M+T) and silica-supported ZrO_2 and the results are summarized in Table 10. At the temperatures studied, no diisopropyl ether was observed over ZrO_2(M+T). As the temperature increased from 513 K to 548 K, the selectivity towards propene increased from 77% to 84% and the selectivity to acetone decreased from 23% to 16%. A different trend was observed over $4ZrO_2/SiO_2$. The overall selectivity to propene increased from 84% to 91% as the temperature increased from 473 K to 523 K and the selectivity to acetone increased as well from 3% to 6%. Unlike ZrO_2(M+T), diisopropyl ether was observed over $4ZrO_2/SiO_2$, and the selectivity towards diisopropyl ether decreased from 13% to 3% as the temperature increased.

Table 10. Decomposition of 2-propanol over ZrO_2(M+T) and $4ZrO_2/SiO_2$.

Catalyst	Temperature (K)	Conversion (%)	Rate x 10^{-4} (mol (mol Zr)$^{-1}$ s^{-1})	Selectivity (%)		
				Propene	Acetone	Diisopropyl Ether
ZrO_2(M+T)	513	7.0	0.42	77	23	-
ZrO_2(M+T)	523	6.4	0.59	76	24	-
ZrO_2(M+T)	548	7.2	8.8	84	16	-
$4ZrO_2/SiO_2$	473	5.9	7.6	84	3	13
$4ZrO_2/SiO_2$	498	8.6	54	86	7	7
$4ZrO_2/SiO_2$	513	8.5	81	88	8	4
$4ZrO_2/SiO_2$	523	7.3	140	91	6	3

Reaction conditions: 5 kPa 2-propanol

The bulk ZrO_2 was more selective to acetone compared to the silica-supported ZrO_2, most likely due to the difference in basic sites, and there was a significant difference in the rate of 2-propanol decomposition over the two catalysts. At the same temperature of 513 K, the rate of reaction was 4.2×10^{-5} mol (mol Zr)$^{-1}$ s^{-1} over ZrO_2(M+T) and 8.1×10^{-3} mol (mol Zr)$^{-1}$ s^{-1} over $4ZrO_2/SiO_2$, a factor of two orders of magnitude. The effect of temperature, at these reaction conditions, appears to be more significant on the $4ZrO_2/SiO_2$ compared to ZrO_2(M+T) as well.

The conversion, rate, and selectivity during 2-propanol decomposition over ZrO_2/SiO_2 catalyst with different ZrO_2 loadings are summarized in Table 11. At a similar conversion of 2-propanol, the observed rate (shown here as a turnover frequency) was similar over the catalysts with ZrO_2 weight loadings that ranged from 4 to 16 wt%. Likewise, the product distribution was nearly independent of loading. As the turnover frequency was independent of weight loading, the results are consistent with a very high fraction of Zr being available for catalysis.

Table 11. Decomposition of 2-propanol over silica-supported ZrO_2 catalysts.

Catalyst	Conversion (%)	Rate x 10^{-3} (mol (mol Zr)$^{-1}$ s^{-1})	Selectivity (%)		
			Propene	Acetone	Diisopropyl Ether
$4ZrO_2/SiO_2$	7.8	1.0	80	8	12
$8ZrO_2/SiO_2$	11	1.4	85	5	10
$16ZrO_2/SiO_2$	8.3	1.1	77	10	13

Reaction conditions: 5 kPa 2-propanol, 473 K

Hydrogen Transfer from Ethanol to Acetone

The hydrogenation of acetone with H_2 was not observed over ZrO_2 based catalysts in this work (results not shown). Therefore, we used the hydrogen transfer of ethanol to acetone to study silica-supported ZrO_2, ZrO_2(M), ZrO_2(M+T), and $1Ag/4ZrO_2/SiO_2$.

Figure 12 shows the rate of 2-propanol formation from the MPV-like hydrogen transfer reaction from ethanol to acetone over $4ZrO_2/SiO_2$, $1Ag/4ZrO_2/SiO_2$, ZrO_2(M), and ZrO_2(M+T) over a range of acetone/ethanol pressures (molar ratio of acetone to ethanol held constant at 0.1). The rate of 2-propanol formation was similar over $4ZrO_2/SiO_2$ and $1Ag/4ZrO_2/SiO_2$ indicating that the addition of Ag did not contribute significantly to the 2-propanol formation. Bulk ZrO_2 had a much lower 2-propanol formation rate compared to the silica-supported ZrO_2 catalysts, indicating that ZrO_2/SiO_2 is much more effective at hydrogenating acetone with ethanol. A study conducted by Sushkevich et al. compared ZrO_2 supported on SiO_2 (1.4 wt% Zr) with bulk ZrO_2 in the MPV-like reaction of crotonaldehyde with ethanol.[56] They concluded that the rate of the MPV-like reaction was higher on bulk ZrO_2. The rates from that particular study, however, were based on the mass of the catalyst (i.e., per gram of catalyst). For a supported catalyst such as ZrO_2/SiO_2, it is likely that most of the support surface is not involved in the MPV-like reaction and is therefore more informative to compare rates based on the exposed Zr atoms present on the catalyst surface. When the rates reported by Sushkevich et al. were evaluated per estimated Zr surface atom

(see Supporting Information), the rate of the MPV-like reaction was actually higher on their ZrO_2/SiO_2 compared to their bulk ZrO_2, which is consistent with the observations in our work with ethanol and acetone (Figure 12).

The trends observed with the various probe reactions provide insights into why silica-supported ZrO_2 is superior to bulk ZrO_2 in the cascade reaction of ethanol to butadiene. Depending on the sample, bulk ZrO_2 can be too reactive with ethanol favoring the unselective dehydration reaction to ethene and diethyl ether (Table 5). As described in Scheme 2a, important steps in the formation of butadiene include hydrogen transfer after aldol condensation and dehydration of intermediates to butadiene. Although H_2 (from ethanol dehydrogenation) may contribute slightly to the hydrogenation of intermediates over the Ag catalysts, we know that the MPV-like hydrogen transfer can be important in the cascade reaction. Figure 12 illustrates the substantially higher effectiveness of silica-supported ZrO_2 for the MPV-like hydrogen transfer compared to bulk ZrO_2. Regarding the dehydration

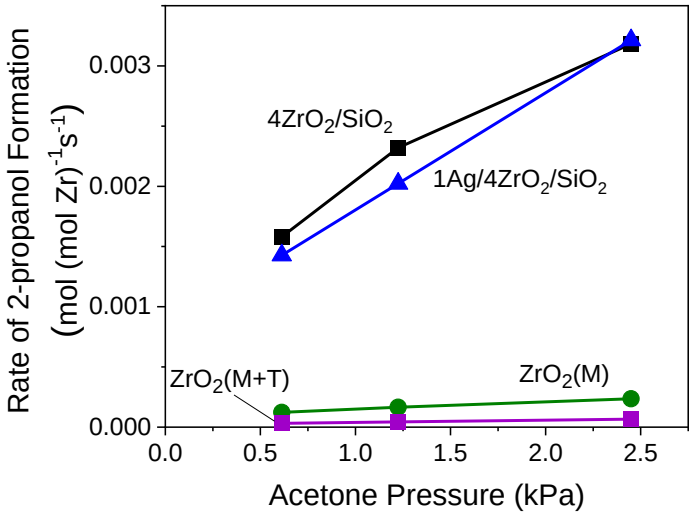

Figure 12. The rate of 2-propanol formation for the MPV-like reaction of ethanol and acetone (molar ratio of acetone to ethanol of 0.1) at 473 K for ZrO_2(M+T), ZrO_2(M), $1Ag/4ZrO_2/SiO_2$, and $4ZrO_2/SiO_2$.

reactions, the very high rate of 2-propanol dehydration over silica-supported ZrO_2 relative to bulk ZrO_2(M+T), as summarized in Table 10, is opposite that observed with ethanol dehydration (Table 5). Evidently, the relative reactivity of the ZrO_2 catalysts for alcohol dehydration reactions depends significantly on the structure of the alcohol. Bulk ZrO_2 is apparently more effective at dehydrating a primary alcohol (ethanol) whereas silica-supported ZrO_2 is more effective at dehydrating a secondary alcohol (2-propanol), which is generally considered easier to dehydrate than a primary alcohol. As butadiene has a conjugated double bond system, we suspect that dehydration of surface intermediate alcohols leading to butadiene would also be facile on the silica-supported ZrO_2 catalysts. Finally, the stronger basic sites present on the bulk ZrO_2 samples, as determined from the 1-butene isomerization results and CO_2 DRIFTS experiments, likely affects the product distribution during ethanol reactions. Indeed, comparison of Figures 11(a) and 11(b) show that bulk ZrO_2 is less effective than silica-supported ZrO_2 at forming butadiene relative to other C4 and higher products. In summary, the silica-supported ZrO_2 catalysts expose appropriate active sites for various transformations in the cascade reaction of ethanol to butadiene compared to bulk ZrO_2.

Conclusion

A physical mixture of silica-supported Ag and ZrO_2 was found to have similar catalytic performance to a co-impregnated catalyst ($1Ag/4ZrO_2/SiO_2$) in the ethanol-to-butadiene reaction. Using a physical mixture, the performance of silica-supported ZrO_2 and bulk ZrO_2 was compared by varying the Ag to ZrO_2 ratio in the catalyst bed. Both sets of physical mixtures showed a similar trend, with butadiene selectivity reaching a clear maximum as the

ratio of Ag to ZrO_2 was varied. The similar butadiene selectivity trend observed for the silica-supported ZrO_2 and bulk ZrO_2 indicates that a proper balance needs to exist between the Ag and ZrO_2 in the catalyst bed in order to achieve the highest butadiene selectivity, since Ag catalyzes the dehydrogenation of ethanol while ZrO_2 catalyzes the C-C coupling and dehydration. The physical mixture of $1Ag/SiO_2$ with either ZrO_2/SiO_2 or bulk ZrO_2 also revealed that the silica-supported ZrO_2 was more effective than bulk ZrO_2 at producing butadiene. Likewise, the rate of the MPV-like hydrogen transfer from ethanol to acetone was significantly higher on the supported ZrO_2 compared to bulk ZrO_2.

The acid-base nature of silica-supported ZrO_2 versus bulk ZrO_2 was explored using adsorbed probe molecules and catalytic probe reactions. Characterization with CO and pyridine indicates that both bulk ZrO_2 and supported ZrO_2 expose Lewis acid sites, with only trace Brønsted acid sites being detected. Results from CO_2 DRIFTS/TPD and the double-bond isomerization of 1-butene revealed that the basic sites on bulk ZrO_2, presumably associated with surface oxygen anions, seem to be stronger compared to silica-supported ZrO_2. The combination of reactivity results from catalytic probe reactions and various catalyst characterization methods shows that the nature of ZrO_2 dispersed on silica is beneficial for the cascade reaction of ethanol to butadiene relative to bulk ZrO_2 under identical conditions.

Conflict of Interest

All authors declare that they have no conflict of interest.

Supporting Information

The Supporting Information is available free of charge at [Link provided by publisher]

Characterization details of ZrO_2 and ZrO_2/SiO_2: X-ray diffraction patterns, Raman spectra, sample Tauc plot, UV-vis spectra, XANES, EXAFS, adsorption microcalorimetry, DRIFTS; additional experimental results from the ethanol reaction, 1-butene isomerization, and 2-propanol decomposition; equilibrium conversion of ethanol dehydrogenation; and sample calculations for Ag dispersion, internal mass transport limitation, and crotyl alcohol formation rates.

Acknowledgements

This work was supported by the U.S. Department of Energy, Office of Science, Basic Energy Sciences, Catalysis Science Program, under Award # DE-FG02-95ER14549. RJD would like to acknowledge the many insightful discussions and productive research collaborations with Professor James Dumesic regarding the catalytic conversion of biomass-derived resources. Dr. Eli Stavitski is acknowledged for his assistance in collecting X-ray absorption spectra. This research used beamline 8-ID (ISS) of the National Synchrotron Light Source II, a U.S. Department of Energy (DOE) Office of Science User Facility operated for the DOE Office of Science by Brookhaven National Laboratory under Contract No. DE-SC0012704.

References

[1] E. V Makshina;M. Dusselier;W. Janssens;J. Degrève;P. A. Jacobs;B. F. Sels, "Review of old chemistry and new catalytic advances in the on-purpose synthesis of butadiene.," *Chem. Soc. Rev.*, **2014**, 43, (22), 7917–7953, doi: 10.1039/c4cs00105b.

[2] C. Angelici;B. M. Weckhuysen;P. C. A. Bruijnincx, "Chemocatalytic conversion of ethanol into butadiene and other bulk chemicals," *ChemSusChem*, **2013**, 6, (9), 1595–

1614, doi: 10.1002/cssc.201300214.

[3] G. Pomalaza;P. Arango Ponton;M. Capron;F. Dumeignil, "Ethanol-to-butadiene: The reaction and its catalysts," *Catal. Sci. Technol.*, **2020**, 10, (15), 4860–4911, doi: 10.1039/d0cy00784f.

[4] G. Pomalaza;M. Capron;V. Ordomsky;F. Dumeignil, "Recent Breakthroughs in the Conversion of Ethanol to Butadiene," *Catalysts*, **2016**, 6, (12), 203, doi: 10.3390/catal6120203.

[5] A. D. Patel;K. Meesters;H. den Uil;E. de Jong;K. Blok;M. K. Patel, "Sustainability assessment of novel chemical processes at early stage : application to biobased processes," *Energy Environ. Sci.*, **2012**, 5, 8430–8444, doi: 10.1039/c2ee21581k.

[6] D. Cespi;F. Passarini;I. Vassura;F. Cavani, "Butadiene from biomass, a life cycle perspective to address sustainability in the chemical industry," *Green Chem.*, **2016**, 18, 1625–1638, doi: 10.1039/c5gc02148k.

[7] S. Shylesh;A. A. Gokhale;C. D. Scown;D. Kim;C. R. Ho;A. T. Bell, "From Sugars to Wheels: The Conversion of Ethanol to 1,3-Butadiene over Metal-Promoted Magnesia-Silicate Catalysts," *ChemSusChem*, **2016**, 9, (12), 1462–1472, doi: 10.1002/cssc.201600195.

[8] J. N. Chheda;G. W. Huber;J. A. Dumesic, "Liquid-phase catalytic processing of biomass-derived oxygenated hydrocarbons to fuels and chemicals," *Angew. Chemie - Int. Ed.*, **2007**, 46, (38), 7164–7183, doi: 10.1002/anie.200604274.

[9] J. C. Serrano-Ruiz;J. A. Dumesic, "Catalytic routes for the conversion of biomass into liquid hydrocarbon transportation fuels," *Energy Environ. Sci.*, **2011**, 4, (1), 83–99, doi: 10.1039/c0ee00436g.

[10] D. M. Alonso;J. Q. Bond;J. A. Dumesic, "Catalytic conversion of biomass to biofuels,"

Green Chem., **2010**, 12, (9), 1493–1513, doi: 10.1039/c004654j.

[11] J. T. Prillaman;N. Miyake;R. J. Davis, "Calcium Phosphate Catalysts for Ethanol Coupling to Butanol and Butadiene," *Catal. Letters*, **2020**, (151), 648–657, doi: 10.1007/s10562-020-03342-5.

[12] W. J. Toussaint;J. T. Dunn;D. R. Jachson, "Production of Butadiene from Alcohol," *Ind. Eng. Chem.*, **1947**, 39, (2), 120–125, doi: 10.1021/ie50446a010.

[13] R. Natta;G. Rigamonti, "X-ray and chemical examination of catalysts used in the manufacture of butadiene from alcohol," *Chim. Ind.*, **1947**, 29, 239–243.

[14] M. D. Jones;C. G. Keir;C. Di Iulio;R. A. M. Robertson;C. V. Williams;D. C. Apperley, "Investigations into the conversion of ethanol into 1,3-butadiene," *Catal. Sci. Technol.*, **2011**, 1, (2), 267–272, doi: 10.1039/c0cy00081g.

[15] E. V. Makshina;W. Janssens;B. F. Sels;P. A. Jacobs, "Catalytic study of the conversion of ethanol into 1,3-butadiene," *Catal. Today*, **2012**, 198, (1), 338–344, doi: 10.1016/j.cattod.2012.05.031.

[16] C. Angelici;M. E. Z. Velthoen;B. M. Weckhuysen;P. C. A. Bruijnincx, "Effect of preparation method and CuO promotion in the conversion of ethanol into 1,3-butadiene over SiO_2-MgO catalysts," *ChemSusChem*, **2014**, 7, (9), 2505–2515, doi: 10.1002/cssc.201402361.

[17] W. E. Taifan;Y. Li;J. P. Baltrus;L. Zhang;A. I. Frenkel;J. Baltrusaitis, "Operando Structure Determination of Cu and Zn on Supported MgO/SiO_2 Catalysts during Ethanol Conversion to 1,3-Butadiene," *ACS Catal.*, **2019**, 9, (1), 269–285, doi: 10.1021/acscatal.8b03515.

[18] D. D. Petrolini;N. Eagan;M.R. Ball;S.P. Burt;I. Hermans;G.W. Huber;J.A. Dumesic;L.

Martins, “Ethanol condensation at elevated pressure over copper on AlMgO and AlCaO porous mixed-oxide supports,” *Catal. Sci. Technol.*, **2019**, 9, (8), 2032–2042, doi: 10.1039/c9cy00316a.

[19] V. L. Dagle;M. D. Flake;T. L. Lemmon;J. S. Lopez;L. Kovarik; R. A. Dagle, “Effect of the SiO_2 support on the catalytic performance of $Ag/ZrO_2/SiO_2$catalysts for the single-bed production of butadiene from ethanol,” *Appl. Catal. B Environ.*, **2018**, 236, 576–587, doi: 10.1016/j.apcatb.2018.05.055.

[20] V. L. Sushkevich;I. I. Ivanova;V. V. Ordomsky;E. Taarning, “Design of a metal-promoted oxide catalyst for the selective synthesis of butadiene from ethanol,” *ChemSusChem*, **2014**, 7, (9), 2527–2536, doi: 10.1002/cssc.201402346.

[21] S. A. Akhade;A. Winkelman;V.L. Dagle;L. Kovarik;S.F. Yuk;M-S Lee;J. Zhang;A.B. Padmaperuma;R.A. Dagle;V-A. Glezakou;Y. Wang;R. Rousseau, “Influence of Ag metal dispersion on the thermal conversion of ethanol to butadiene over $Ag\text{-}ZrO_2/ SiO_2$ catalysts,” *J. Catal.*, **2020**, 386, 30–38, doi: 10.1016/j.jcat.2020.03.030.

[22] Y. Zhao;W. Li;M. Zhang;K. Tao, “A comparison of surface acidic features between tetragonal and monoclinic nanostructured zirconia,” *Catal. Commun.*, **2002**, 3, (6), 239–245, doi: 10.1016/S1566-7367(02)00089-4.

[23] K. Tanabe, “Surface and catalytic properties of ZrO_2,” *Mater. Chem. Phys.*, **1985**, 13, (3–4), 347–364, doi: 10.1016/0254-0584(85)90064-1.

[24] B. Bachiller-Baeza;I. Rodriguez-Ramos;A. Guerrero-Ruiz, “Interaction of carbon dioxide with the surface of zirconia polymorphs,” *Langmuir*, **1998**, 14, (13), 3556–3564, doi: 10.1021/la970856q.

[25] K. T. Jung;A. T. Bell, “Effects of zirconia phase on the synthesis of methanol over

zirconia-supported copper," *Catal. Lett.*, **2002**, 80, (1–2), 63–68.

[26] V. L. Sushkevich;I. I. Ivanova, "Mechanistic study of ethanol conversion into butadiene over silver promoted zirconia catalysts," *Appl. Catal. B Environ.*, **2017**, 215, 36–49, doi: 10.1016/j.apcatb.2017.05.060.

[27] V. L. Sushkevich;D. Palagin;I. I. Ivanova, "With Open Arms: Open Sites of ZrBEA Zeolite Facilitate Selective Synthesis of Butadiene from Ethanol," *ACS Catal.*, **2015**, 5, (8), 4833–4836, doi: 10.1021/acscatal.5b01024.

[28] V. L. Sushkevich;I. I. Ivanova;E. Taarning, "Ethanol conversion into butadiene over Zr-containing molecular sieves doped with silver," *Green Chem.*, **2015**, 17, (4), 2552–2559, doi: 10.1039/C4GC02202E.

[29] G. Brezicki;J. Zheng;C. Paolucci;R. Schlögl;R. J. Davis, "Effect of the Co-cation on Cu Speciation in Cu-Exchanged Mordenite and ZSM-5 Catalysts for the Oxidation of Methane to Methanol," *ACS Catal.*, **2021**, (11), 4973–4987, doi: 10.1021/acscatal.1c00543.

[30] G. Brezicki;J. D. Kammert;T. B. Gunnoe;C. Paolucci;R. J. Davis, "Insights into the Speciation of Cu in the Cu-H-Mordenite Catalyst for the Oxidation of Methane to Methanol," *ACS Catal.*, **2019**, 9, (6), 5308–5319, doi: 10.1021/acscatal.9b00852.

[31] B. Ravel;M. Newville, "ATHENA , ARTEMIS , HEPHAESTUS : data analysis for X-ray absorption spectroscopy using IFEFFIT," *J. Synchrotron Radiat.*, **Jul. 2005**, 12, (4), 537–541, doi: 10.1107/S0909049505012719.

[32] J. D. Kammert;G. Brezicki;R. Acevedo-Esteves;E. Stavitski;R. J. Davis, "High-throughput operando -ready X-ray absorption spectroscopy flow reactor cell for powder samples," *Rev. Sci. Instrum.*, **2020**, 91, (1), doi: 10.1063/1.5124301.

[33] X. Gao;J. L. G. Fierro;I. E. Wachs, “Structural characteristics and catalytic properties of highly dispersed ZrO_2/SiO_2 and $V_2O_5/ZrO_2/SiO_2$ catalysts,” *Langmuir*, **1999**, 15, (9), 3169–3178, doi: 10.1021/la981254p.

[34] C. K. Kwok;C. R. Aita, “Near-band gap optical behavior of sputter deposited α- and α+β-ZrO2 films,” *J. Appl. Phys.*, **1989**, 66, (6), 2756–2758, doi: 10.1063/1.344484.

[35] S. C. Moon;M. Fujino;H. Yamashita;M. Anpo, “Characterization of zirconium-silicon binary oxide catalysts prepared by the sol-gel method and their photocatalytic activity for the isomerization of 2-butene,” *J. Phys. Chem. B*, **1997**, 101, (3), 369–373, doi: 10.1021/jp961523p.

[36] E. Fernandez Lopez;V. Sanchez Escribano;M. Panizza;M. M. Carnasciali;G. Busca, “Vibrational and electronic spectroscopic properties of zirconia powders,” *J. Mater. Chem.*, **2001**, 11, (7), 1891–1897, doi: 10.1039/b100909p.

[37] G. Mountjoy;D.M. Pickup;R. Anderson;G.W. Wallidge;M.A. Holland;R.J. Newport;M.E. Smith, “Changes in the Zr environment in zirconia-silica xerogels with composition and heat treatment as revealed by Zr K-edge XANES and EXAFS,” *Phys. Chem. Chem. Phys.*, **2000**, (10), 2455–2460.

[38] P. Li;I. Chen, “X-ray absorption studies of zirconia polymorphs. I. Characteristic local structures,” *Phys. Rev. B*, **1993**, 48, (14), 63–73.

[39] F. Meneghetti;E. Wendel;S. Mascotto;B.M. Smarsly;E. Tondello;H. Bertagnolli;S. Gross, “Combined use of XAFS, XRD and TEM to unravel the microstructural evolution of nanostructured ZrO_2-SiO_2 binary oxides: From nanometres down to the molecular domain,” *CrystEngComm*, **2010**, 12, (5), 1639–1649, doi: 10.1039/b911004f.

[40] W. C. Vining;J. Strunk;A. T. Bell, “Investigation of the structure and activity of

$VO_x/ZrO_2/SiO_2$ catalysts for methanol oxidation to formaldehyde," *J. Catal.*, **2011**, 281, (2), 222–230, doi: 10.1016/j.jcat.2011.05.001.

[41] I. M. Hill;S. Hanspal;Z. D. Young;R. J. Davis, "DRIFTS of Probe Molecules Adsorbed on Magnesia, Zirconia, and Hydroxyapatite Catalysts," *J. Phys. Chem. C*, **2015**, 119, (17), 9186–9197, doi: 10.1021/jp509889j.

[42] E. P. Parry, "An Infrared Study of Pyridine adsorbed on acidic solids. Characterization of surface acidity," *J. Catal.*, **1963**, 2, 371–379.

[43] H. Li;J. Pang;N.R. Jaegers;L. Kovarik;M. Engelhard;A.W. Savoy;J. Hu;J. Sun;Y. Wang, "Conversion of ethanol to 1,3–butadiene over Ag–ZrO_2/SiO_2 catalysts: The role of surface interfaces," *J. Energy Chem.*, **2020**, 54, 7–15, doi: 10.1016/j.jechem.2020.05.038.

[44] J. E. Tábora;R. J. Davis, "Structure of Fe, Mn-promoted sulfated zirconia catalyst by X-ray and IR absorption spectroscopies," *J. Chem. Soc. Faraday Trans.*, **1995**, 91, (12), 1825–1833, doi: 10.1039/FT9959101825.

[45] K. I. Hadjiivanov;G. N. Vayssilov, "Characterization of oxide surfaces and zeolites by carbon monoxide as an IR probe molecule," *Adv. Catal.*, **2002**, 47, 307–511, doi: 10.1016/S0360-0564(02)47008-3.

[46] C. Morterra;R. Aschieri;M. Volante, "Surface Characterization of Zirconium Oxide. I. Surface Activation and the Development of a Strong Lewis Acidity," *Mater. Chem. Phys.*, **1988**, 20, 539–557.

[47] C. Morterra;L. Orio, "Surface characterization of zirconium oxide. II. The interaction with carbon dioxide at ambient temperature," *Mater. Chem. Phys.*, **1990**, 24, (3), 247–268, doi: 10.1016/0254-0584(90)90089-S.

[48] V. L. Sushkevich;I. I. Ivanova;E. Taarning, "Mechanistic study of ethanol dehydrogenation over silica-supported silver," *ChemCatChem*, **2013**, 5, (8), 2367–2373, doi: 10.1002/cctc.201300033.

[49] G. Garbarino;P. Riani;M. Villa García;E. Finocchio;V. Sanchez Escribano;G. Busca, "A study of ethanol dehydrogenation to acetaldehyde over copper/zinc aluminate catalysts," *Catal. Today*, **2020**, 354, 167–175, doi: 10.1016/j.cattod.2019.01.002.

[50] G. Garbarino;G. Pampararo;T. K. Phung;P. Riani;G. Busca, "Heterogeneous catalysis in (bio)ethanol conversion to chemicals and fuels: Thermodynamics, catalysis, reaction paths, mechanisms and product selectivities," *Energies*, **2020**, 13, (14), doi: 10.3390/en13143587.

[51] C. T. Fishel;R. J. Davis, "Use of catalytic reactions to probe Mg-Al mixed oxide surfaces," *Catal. Letters*, **1994**, 25, (1–2), 87–95, doi: 10.1007/BF00815418.

[52] A. Gervasini;A. Auroux, "Acidity and Basicity of Metal Oxide Surfaces II. Determination by Catalytic Decomposition of Isopropanol," *J. Catal.*, **1991**, 131, 190–198, doi: 10.1016/0021-9517(91)90335-2.

[53] D. Kulkarni;I. E. Wachs, "Isopropanol oxidation by pure metal oxide catalysts: Number of active surface sites and turnover frequencies," *Appl. Catal. A Gen.*, **2002**, 237, (1–2), 121–137, doi: 10.1016/S0926-860X(02)00325-3.

[54] Z. D. Young;R. J. Davis, "Hydrogen transfer reactions relevant to Guerbet coupling of alcohols over hydroxyapatite and magnesium oxide catalysts," *Catal. Sci. Technol.*, **2018**, 8, (6), 1722–1729, doi: 10.1039/c7cy01393k.

[55] T. Moteki;D. W. Flaherty, "Mechanistic Insight to C-C Bond Formation and Predictive Models for Cascade Reactions among Alcohols on Ca- and Sr-Hydroxyapatites," *ACS*

Catal., **2016**, 6, (7), 4170–4183, doi: 10.1021/acscatal.6b00556.

[56] V. L. Sushkevich;I. I. Ivanova;S. Tolborg;E. Taarning, "Meerwein-Ponndorf-Verley-Oppenauer reaction of crotonaldehyde with ethanol over Zr-containing catalysts," *J. Catal.*, **2014**, 316, 121–129, doi: 10.1016/j.jcat.2014.04.019.

[57] A. Ozaki;K. Kimura, "The effective site on acid catalysts revealed in n-butene isomerization," *J. Catal.*, **1964**, 3, (5), 395–405, doi: 10.1016/0021-9517(64)90142-3.

[58] Y. Nakano;T. Iizuka;H. Hattori;K. Tanabe, "Surface properties of zirconium oxide and its catalytic activity for isomerization of 1-butene," *J. Catal.*, **1979**, 57, (1), 1–10, doi: 10.1016/0021-9517(79)90038-1.

[59] M. J. Baird;J. H. Lunsford, "Catalytic sites for the isomerization of 1-butene over magnesium oxide," *J. Catal.*, **1972**, 26, (3), 440–450, doi: 10.1016/0021-9517(72)90105-4.

For Table of Contents Use Only

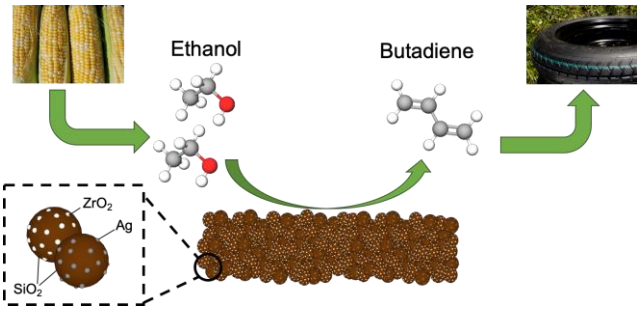

Synopsis

Conversion of bio-ethanol to butadiene may lower greenhouse gas emissions compared to conventional butadiene production from fossil resources, provided effective catalysts are discovered.